Cell Reports

Article

The STRIPAK complex is required for radial sorting and laminin receptor expression in Schwann cells

Graphical abstract

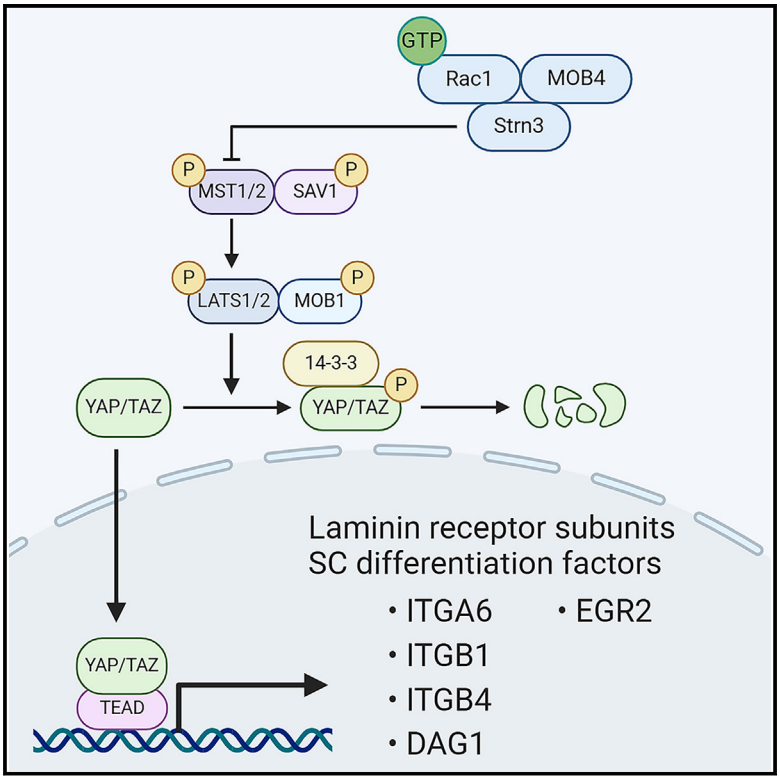

Highlights

- YAP/TAZ-mediated gene transcription is necessary for Schwann cell development
- The STRIPAK complex regulates Schwann cell YAP/TAZ activity and laminin receptor expression
- STRIPAK members STRN3 and MOB4 directly interact with active RAC1-GTP
- *Rac1* ablation in Schwann cells causes dysregulation of YAP/TAZ

Authors

Michael R. Weaver, Dominika Shkoruta, Marta Pellegatta, ..., Fraser Sim, Yannick Poitelon, M. Laura Feltri

Correspondence

mweaver2@buffalo.edu (M.R.W.), poitely@amc.edu (Y.P.)

In brief

YAP/TAZ-mediated gene transcription is necessary for Schwann cell laminin receptor expression and differentiation. Weaver et al. use transgenic mouse models to show that the STRIPAK complex is required to regulate YAP/TAZ and facilitate radial sorting. Additionally, they show that two STRIPAK complex members, STRN3 and MOB4, directly interact with Rac1-GTP.

Weaver et al., 2025, Cell Reports *44*, 115401
March 25, 2025
https://doi.org/10.1016/j.celrep.2025.115401

CellPress

Cell Reports

CellPress
OPEN ACCESS

Article

The STRIPAK complex is required for radial sorting and laminin receptor expression in Schwann cells

Michael R. Weaver,[1,*] Dominika Shkoruta,[2] Marta Pellegatta,[1,3] Caterina Berti,[1,3] Marilena Palmisano,[1,3] Scott Ferguson,[1,4] Edward Hurley,[1] Julianne French,[7] Shreya Patel,[7] Sophie Belin,[7] Matthias Selbach,[5] Florian Ernst Paul,[5] Fraser Sim,[6] Yannick Poitelon,[7,10,*] and M. Laura Feltri[1,3,8,9]

[1]Institute for Myelin and Glia Exploration, Buffalo, NY, USA
[2]Ivano-Frankivsk National Medical University, Ivano-Frankivsk, Ivano-Frankivsk Oblast, Ukraine
[3]Department of Biochemistry, Buffalo, NY, USA
[4]Department of Pharmaceutical Sciences, Buffalo, NY, USA
[5]Max Delbrück Center for Molecular Medicine, Berlin, Germany
[6]Department of Pharmacology and Toxicology, Buffalo, NY, USA
[7]Department of Neuroscience and Experimental Therapeutics, Albany Medical College, Albany, NY, USA
[8]Department of Neurology, State University of New York at Buffalo Jacob's School of Medicine and Biomedical Sciences, Buffalo, NY, USA
[9]Deceased
[10]Lead contact
*Correspondence: mweaver2@buffalo.edu (M.R.W.), poitely@amc.edu (Y.P.)
https://doi.org/10.1016/j.celrep.2025.115401

SUMMARY

During peripheral nervous system development, Schwann cells undergo Rac1-dependent cytoskeletal reorganization as they insert cytoplasmic extensions into axon bundles to sort and myelinate individual axons. However, our understanding of the direct effectors targeted by Rac1 is limited. Here, we demonstrate that striatin-3 and MOB4 are Rac1 interactors. We show that Schwann-cell-specific ablation of striatin-3 causes defects in lamellipodia formation, and conditional Schwann cell knockout for striatins presents a severe delay in radial sorting. Finally, we demonstrate that deletion of Rac1 or striatin-1/3 in Schwann cells causes defects in the activation of Hippo pathway effectors YAP and TAZ and the expression of genes co-regulated by YAP and TAZ, such as extracellular matrix receptors. In summary, our results indicate that striatin-3 is a Rac1 interactor and that striatins are required for peripheral nervous system development and reveal a role for Rac1 in the regulation of the Hippo pathway in Schwann cells.

INTRODUCTION

Radial sorting of axons by Schwann cells (SCs) in the peripheral nervous system (PNS) is a prerequisite for their proper myelination. Failure of radial sorting results in profound developmental defects. Surprisingly, most of the molecules that have been implicated in the radial sorting process are not at the apical, axoglial (adaxonal) interface but on the basal (abaxonal) side of SCs. Indeed, the laminin-rich extracellular matrix (ECM), ECM receptors, and intracellular signaling triggered by ECM receptor-ligand engagement at the abaxonal interface are essential for SCs to radially sort axons.[1–12]

Signaling from laminin receptors also interacts with other signaling cascades that are essential for SC development. Notably, both remodeling of the actin cytoskeleton and cell polarity are regulated by Rho GTPase family members, and several Rho GTPases, including Rac1 and CDC42, are required for radial sorting.[6,13,14] Rac1 and CDC42 have been shown to regulate the activation of PKA through NF2. Moreover, the expression of dominant-negative NF2 partially rescues radial sorting defects in CDC42 mutant mice but not Rac1 mutant mice.[14,15] This suggests that the radial sorting defects observed in Rac1 mutant mice are mediated by additional mechanisms, and our understanding of the direct effectors targeted by Rac1 during radial sorting remains limited.

We previously showed that the Hippo pathway, a signaling cascade that negatively regulates the activity and nuclear translocation of the transcriptional co-activators YAP and TAZ, is also implicated in SC radial sorting.[16,17] YAP and TAZ notably regulate the expression of several laminin receptors and transcription factors essential for myelination.[17–21] It is well characterized that signals from the Hippo pathway, including from the kinases MST1 and MST2, lead to YAP and TAZ inhibition by phosphorylation and cytosolic sequestration. However, it is unknown what additional mechanisms may regulate YAP and TAZ in SCs.

Here, we sought to identify the downstream effectors of Rac1. We demonstrate that striatin-3 (STRN3), a member of striatin-interacting phosphatase and kinase (STRIPAK) complexes, directly interacts with Rac1. We found that the loss of both STRN1 and STRN3 in SCs leads to a severe delay in radial sorting. Finally, we demonstrate that the loss of Rac1 or STRN1 and STRN3 in SCs leads to dysregulation of the Hippo pathway and altered expression of laminin receptors, thus revealing a previously undescribed role for Rac1 in SCs.

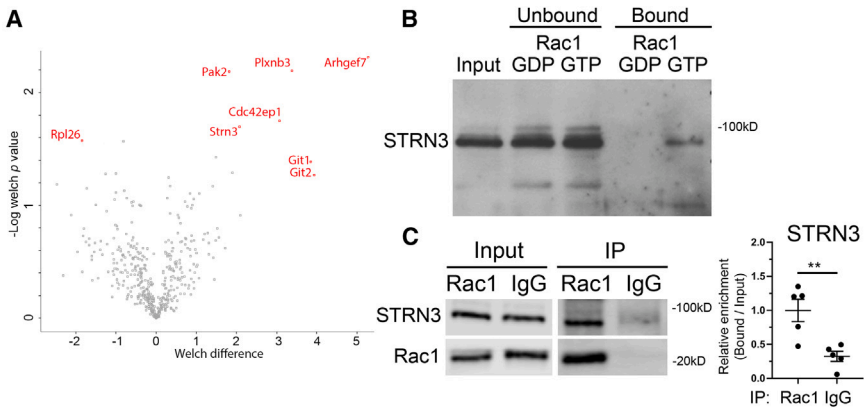

Figure 1. STRN3 interacts directly with Rac1

(A and B) Glutathione S-transferase (GST) pull-down from P5 wild-type (WT) mouse sciatic nerve lysate, comparing GST-Rac1-GDP versus GST-Rac1-GTP.

(A) Volcano plot showing the Welch difference (log2 fold change) of Rac1 interactors. Proteins in red, such as STRN3 and several well-established Rac1 interactors, are significantly (false discovery rate [FDR] = 0.05) enriched in the active Rac1-GTP fraction compared to the inactive Rac1-GDP fraction. MOB4 was found to be enriched in the Rac1-GTP fraction in a separate biological replicate (data not shown).

(B) GST-Rac1-GDP/GTP pull-down of P5 WT sciatic nerve lysate was repeated and analyzed by western blot (WB). STRN3 was observed to elute with the active Rac1-GTP fraction but not the inactive Rac1-GDP fraction.

(C) Immunoprecipitation of Rac1 from SC lysates. STRN3 was found to interact with Rac1 in SCs. $n = 5$ individual coIPs per targeting antibody (anti-Rac1 or IgG isotype control). Unpaired two-tailed t test ($t = 3.730$, df = 8, $p = 0.0058$). Error bars indicate SEM. $^{**}p < 0.01$.

RESULTS

STRN3 and MOB4 both directly interact with Rac1

To screen for candidate Rac1 interactors, we performed a pull-down assay for active versus inactive forms of Rac1 from mouse peripheral nerve lysate at postnatal day 5 (P5), when both radial sorting and myelination are ongoing.[4] Both STRN3 and MOB4, members of the STRIPAK complex, were among the proteins found to be enriched in the active Rac1-GTP fraction (Figures 1A and 1B). We confirmed that this interaction occurred specifically in SCs using both co-immunoprecipitation (coIP) (Figure 1C) and proximity ligation assay (PLA) (Figure S1).

Although the Rac1 pull-down assay, coIP, and PLA experiments strongly suggest that Rac1 associates with STRN3 in tissues and cells, they do not differentiate whether this interaction is direct or indirect. Therefore, we asked if STRN3 or MOB4 binds directly and specifically to Rac1 and in a Rac1-GDP/GTP charge-dependent manner. We used a series of dot blot assays with isolated proteins, which were all independently validated for purity and specificity (Figures S2–S4). We found that both STRN3 and MOB4 bind directly to Rac1 (Figure S5). However, at low concentrations and while isolated from the intracellular milieu, STRN3 exhibits stronger binding to inactive Rac1.

STRN3 is required for SC elongation and process extension

We and others have previously demonstrated that Rac1 inhibition or ablation causes SCs to form fewer lamellipodia, a thin, sheet-like protrusion of the cell membrane that is critical for Rac1-mediated radial sorting and myelination.[6,13,14] Thus, we asked if the loss of STRN3 in SCs may also influence lamellipodia formation and the radial sorting of axons. We generated mice lacking STRN3 in SCs ($Strn3^{SCKO}$; SCKO, SC knockout) using animals expressing Cre recombinase under the control of the SC-specific *Mpz* promoter, which is expressed starting on embryonic day 13.5 (E13.5).[22] We show that SCs isolated from $Strn3^{SCKO}$ mice had little to no STRN3 protein expressed when compared to control SCs (Figures 2A and 2B). Ablation of *Strn3* in SCs did not affect the purity of SC isolation (Figures 2C and 2D) or the adherence of SCs to the substrate *in vitro* (Figure 2E). However, similar to Rac1 inhibition or ablation in SCs, the *Strn3*-null SCs had significantly fewer radial and total lamellipodia per cell (Figures 2C and 2F).[6] We also found that *Strn3*-null SCs had a significant defect in cell elongation (Figures 2C, 2G, and 2H). These data suggest that, like Rac1, STRN3 is a critical regulator of SC cytoskeletal dynamics, specifically cell elongation and lamellipodia formation.

Striatin family protein expression is developmentally regulated

All three striatin proteins share a similar domain structure and a high degree of homology. Additionally, the main known function of each member of the striatin protein family is to act as the center scaffold of STRIPAK complexes.[23–25] Accordingly, we investigated the expression levels of STRN1, STRN3, and STRN4 during key steps of PNS development. Interestingly, the expression of all three striatin proteins followed a very similar pattern in wild-type (WT) peripheral nerves, with high levels of expression early in development, when both radial sorting and myelination are ongoing, and a large, persistent reduction in protein levels after these processes are complete at P20 (Figures 3A and 3B). This suggests that all striatin proteins may have a role in peripheral nerve development and SC biology. In addition, we found that at P10, a time point during which WT mice should be completing radial sorting but are still actively myelinating axons, there is a significant upregulation of STRN4 in sciatic nerves of $Strn3^{SCKO}$ mice (Figures 3C and 3D), suggesting that other striatin proteins may be upregulated to compensate for the loss of STRN3 in SCs during development.

Striatins are essential for SC radial sorting

To determine if the ablation of *Strn3* in SCs causes radial sorting defects, we analyzed electron micrographs and semithin sections of animals lacking one or two members of the striatin family. We found that the loss of any one striatin protein ($Strn1^{SCKO}$, $Strn3^{SCKO}$, or $Strn4^{SCKO}$) resulted in no major defects in the number or density of myelinated fibers or in sciatic

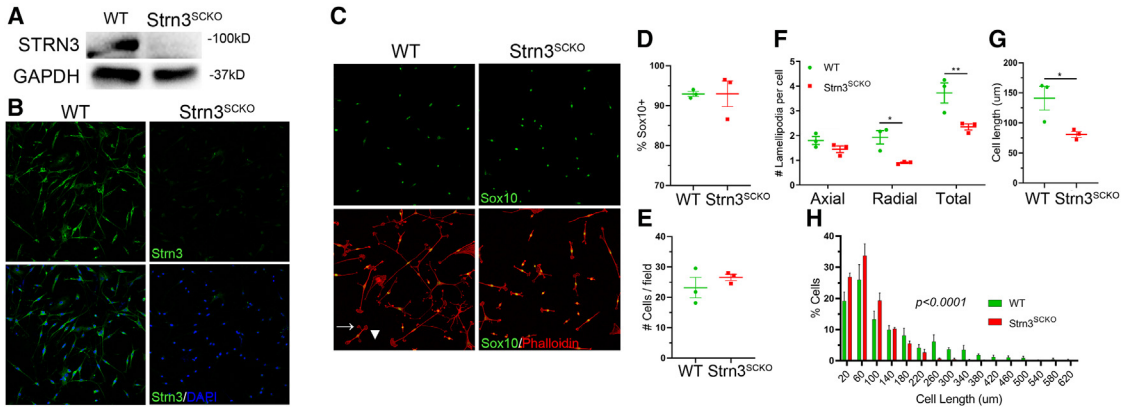

Figure 2. STRN3 is required for SC elongation and lamellipodia formation

SCs were isolated from WT and Strn3^{SCKO} littermates at P45–P60.

(A and B) SCs isolated from Strn3^{SCKO} mice have absent Strn3 protein expression by western blot (A) and immunohistochemistry (B). Similar results were obtained with a second anti-STRN3 antibody (data not shown). STRN3 was stained in green, and nuclei were labeled with DAPI (blue). Scale bar: 20 μm.

(C) Representative immunohistochemistry of mouse SCs, with nuclei labeled with Sox10 (green) and F-actin labeled with phalloidin (red).

(D) Loss of STRN3 in SCs does not alter the purity of SC isolation. Unpaired two-tailed t test (t = 0.01239, df = 4, p = 0.9907).

(E) Deletion of *Strn3* in SCs does not affect the density of SCs adhering to the substrate *in vitro*. Unpaired two-tailed t test (t = 0.9691, df = 4, p = 0.3874).

(F) SCs isolated from Strn3^{SCKO} mice form reduced numbers of radial and total, but not axial, lamellipodia. Axial lamellipodia (white arrowhead) are defined as extending from within a 20° angle of the long axis of the cell, whereas radial lamellipodia (white arrow) protrude from outside of this range. Two-way multiple comparisons ANOVA with Bonferroni post hoc test. F (1,6) genotype = 45.63, p = 0.0005; F (2,6) lamellipodia type = 21.75, p = 0.0018; p_{axial} = 0.5662, p_{radial} = 0.0142, and $p_{axial+radial}$ = 0.0033.

(G and H) SCs ablated for *Strn3* have reduced cell elongation.

(G) Unpaired two-tailed t test (t = 2.978, df = 4, p = 0.0408).

(H) Lognormal nonlinear regression, extra sum-of-squares F test; F (3, 90) = 14.47. n = 3 individual mouse SC isolations per genotype.

Error bars indicate SEM. *p < 0.05 and **p < 0.01.

nerve thickness at P20 (Figures 4C–4F). We investigated Strn3^{SCKO} mice more extensively, and while we identified some very mild radial sorting and myelination defects, myelin thickness was not affected (Figures S6A–S6H). However, the ablation of either *Strn1* or *Strn4* in combination with *Strn3* to produce double SCKO (dSCKO) mice (Strn1/3^{dSCKO} and Strn3/4^{dSCKO}) resulted in a dramatic reduction in the total number and density of myelinated fibers, the presence of immature bundles of unsorted axons, aberrantly myelinated axons inside of unsorted bundles, sorted but amyelinated axons, and thinner, hypoplastic sciatic nerves at P20 (Figure 4). Strn1/3^{dSCKO} mice also retained thinner myelin as late as P60, the latest time point analyzed, suggesting a persistent myelination defect even in SCs that do establish a 1:1 relationship with axons (Figure S7). Strn1/3^{dSCKO} mice were not maintained beyond P60 due to severe, progressive hindlimb muscle wasting and paralysis that began to manifest shortly after P20. While both Strn1/3^{dSCKO} and Strn3/4^{dSCKO} mice had many massive bundles of unsorted, mixed-caliber axons throughout the sciatic nerve (Figure 4), it was Strn1/3^{dSCKO} mice that had the most severe axonal sorting phenotype, which persisted as late as P60. An apparent, though much less severe, axonal sorting phenotype was also observed in sciatic nerves of Strn1/4^{dSCKO} mice (Figure 4). Together, these data suggest that the striatins are essential for SC radial sorting and subsequent myelination during peripheral nerve development and that individual striatin protein family members can partially compensate for the function of the others.

STRN1 and STRN3 are required for Hippo pathway regulation in SCs

The striatin proteins function as the center scaffolds of STRIPAK complexes and are necessary for linking together many other members of the complex.[25] Consistent with this, we found that the deletion of *Strn1* and *Strn3* in SCs alters the protein levels of other STRIPAK complex members, namely MOB4, STRIP1, and CCM3, in both P5 and P20 peripheral nerves (Figure S8). In addition, while we were expecting compensatory upregulation of STRN4 following the loss of STRN1 and STRN3, we found that *Strn4* mRNA and protein levels were also reduced in peripheral nerves of Strn1/3^{dSCKO} mice, suggesting a severe impairment of STRIPAK complexes (Figure S8).

One of the major roles of STRIPAK complexes is to negatively regulate the Hippo pathway, which occurs by dephosphorylation and inactivation of MST1 and MST2 by the STRIPAK-associated PP2A phosphatase.[26–33] Thus, to further explore the mechanisms underlying the developmental defects in peripheral nerves of Strn1/3^{dSCKO} mice, we next asked if the loss of STRN1 and STRN3 and the subsequent reduction in other STRIPAK proteins causes an increase in the phosphorylation of MST1, MST2, YAP, and TAZ. We found that MST1/2 phosphorylation is significantly increased at both P5 and P20 in Strn1/3^{dSCKO} peripheral nerves (Figures 5C–5E). We also observed increased phosphorylation of YAP and TAZ at P20 in Strn1/3^{dSCKO} peripheral nerves (Figures 5C–5E). In addition to these expected results on the phosphorylation of the Hippo pathway, we also found that the absence of STRN1 and STRN3 in SCs led to a decrease in total

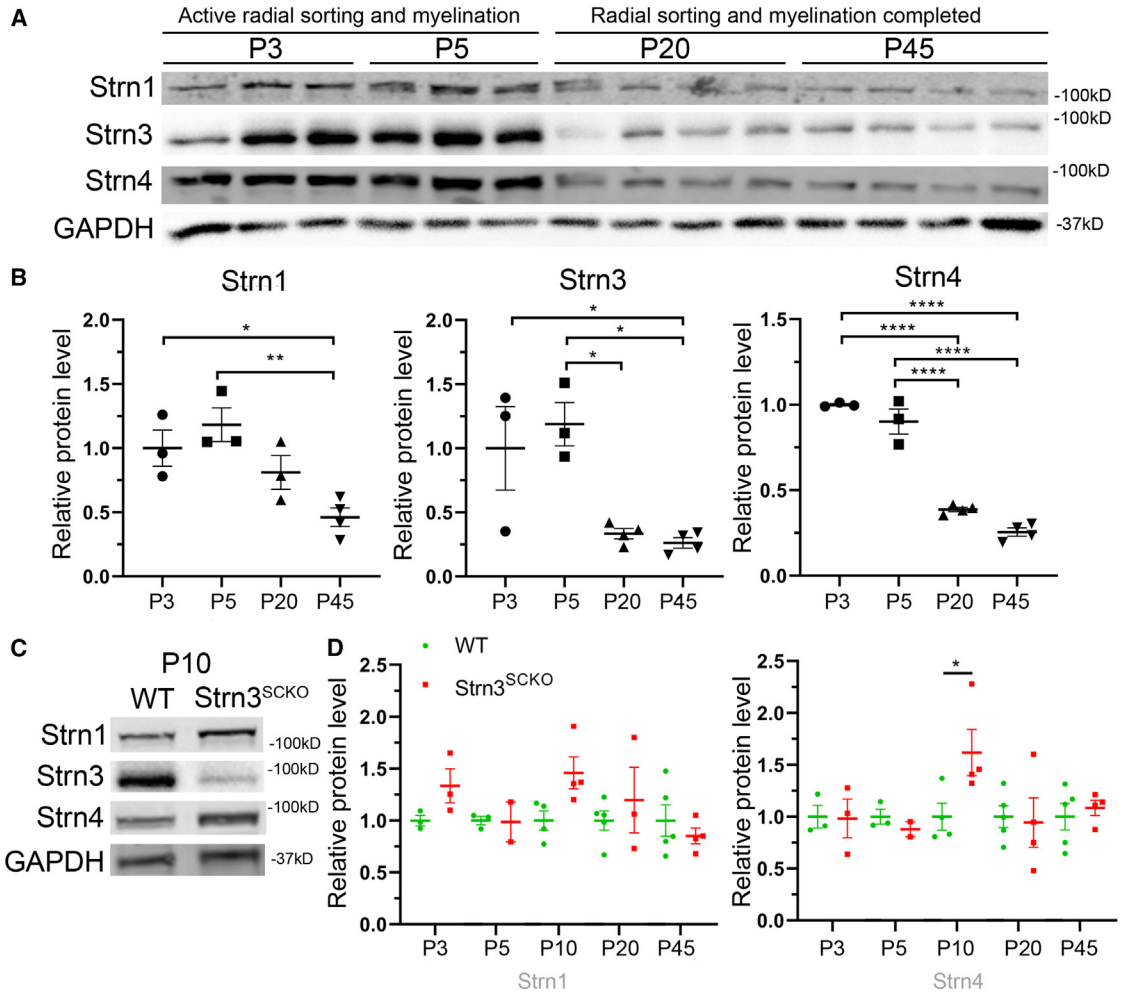

Figure 3. Striatin protein levels are developmentally regulated

(A) STRN1, STRN3, and STRN4 protein levels from WT mouse sciatic nerves at P3, P5, P20, and P45.

(B) Densitometry analysis shows a progressive reduction in STRN1, STRN3, and STRN4 during development in peripheral nerves of WT mice. $n = 3–4$ animals per age group. One-way multiple comparisons ANOVA with Bonferroni post hoc test. STRN1 (F (3,9) = 7.66, $p = 0.0072$, $p_{P3–P5} > 0.9999$, $p_{P3–P20} > 0.9999$, $p_{P3–P45} = 0.0474$, $p_{P5–P20} = 0.3379$, $p_{P5–P45} = 0.0083$, and $p_{P20–P45} = 0.3277$). STRN3 (F (3,10) = 8.772, $p = 0.0038$, $p_{P3–P5} > 0.9999$, $p_{P3–P20} = 0.0813$, $p_{P3–P45} = 0.0471$, $p_{P5–P20} = 0.0196$, $p_{P5–P45} = 0.0117$, and $p_{P20–P45} > 0.9999$). STRN4 (F (3,10) = 113.4, $p < 0.0001$, $p_{P3–P5} = 0.5436$, $p_{P3–P20} < 0.0001$, $p_{P3–P45} < 0.0001$, $p_{P5–P20} < 0.0001$, $p_{P5–P45} < 0.0001$, and $p_{P20–P45} = 0.0939$).

(C) Representative western blots of STRN1, STRN3, and STRN4 from sciatic nerves of WT and Strn3^{SCKO} mice at P10.

(D) Densitometry analysis shows an increase in Strn4 at P10 in peripheral nerves of Strn3^{SCKO} mice. $n = 3–5$ animals per genotype per age group. Two-way multiple comparisons ANOVA with Bonferroni post hoc test. STRN1 (F (4, 15) age = 1.335; $p = 0.3026$; F (1, 11) genotype = 3.755, $p = 0.0787$; $p_{P3} = 0.5333$, $p_{P5} > 0.9999$, $p_{P10} = 0.0896$, $p_{P20} > 0.9999$, and $p_{P45} > 0.9999$). STRN4 (F age (4, 15) = 1.475, $p = 0.2591$; F (1, 12) genotype = 1.305, $p = 0.2755$; $p_{P3} > 0.9999$, $p_{P5} > 0.9999$, $p_{P10} = 0.0190$, $p_{P20} > 0.9999$, and $p_{P45} > 0.9999$).

Error bars indicate SEM. *$p < 0.05$, **$p < 0.01$, and ****$p < 0.0001$.

MST1/2, YAP, and TAZ protein levels at P5 and P20 (Figures 5C–5E). These results were partially correlated to a reduction of *Mst1*, *Mst2*, and *Yap* mRNA levels (Figures 5A and 5B). While it is known that phosphorylation of YAP and TAZ leads to their cytoplasmic retention and subsequent degradation, the global reduction of mRNA and protein levels of various members of the Hippo pathway was unexpected. Together, these data suggest that the loss of STRN1 and STRN3 in SCs causes inhibition of the Hippo pathway via the reduction of gene expression of several Hippo pathway members and through increased phosphorylation of YAP and TAZ, which leads to their cytosolic sequestration and/or degradation.

Rac1 is required for Hippo pathway regulation in SCs

We next sought to clarify if and how Hippo pathway dysfunction in Strn1/3^{dSCKO} mice is related to its interaction with Rac1. First, we found that there were no differences in the activity of Rac1 or CDC42, a related Rho GTPase, or in the phosphorylation of the Rac1 effectors PAK1 or NF2 at P20 in peripheral nerves of Strn1/3^{dSCKO} mice (Figure 6). Thus, our data suggest that

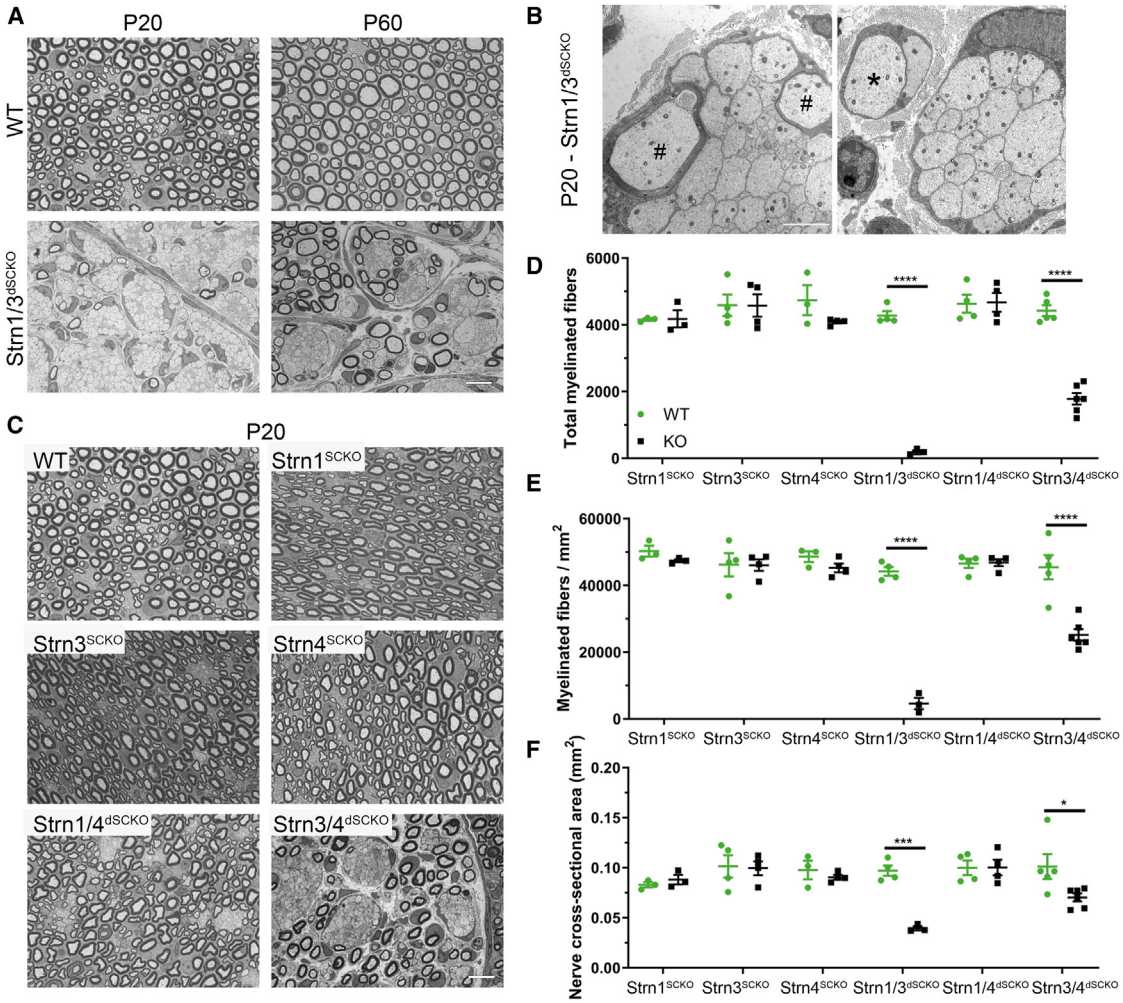

Figure 4. Loss of striatin proteins in SCs results in mild to severe developmental defects

(A–C) Semithin sections (A and C) and electron micrographs (B) of WT and striatin mutant sciatic nerves at P20 (A–C) and P60 (A). At P20, Strn1/3^{dSCKO} nerves present with immature bundles of unsorted axons, myelinated axons inside unsorted bundles (#), and amyelinated axons (*). Scale bars: 10 μm (A and C) and 2 μm (B).

(D–F) At P20, sciatic nerves of Strn1/3^{dSCKO} and Strn3/4^{dSCKO} mice have significantly fewer total myelinated fibers, a lower density of myelinated fibers, and thinner, hypoplastic sciatic nerves. $n = 3$–6 animals per genotype. Two-way multiple comparisons ANOVA with Bonferroni post hoc test. Total fibers (F (5, 35) model = 32.90; $p < 0.0001$; F (1, 35) WT versus KO = 76.14, $p < 0.0001$; $p_{Strn1\text{-}SCKO} > 0.9999$, $p_{Strn3\text{-}SCKO} > 0.9999$, $p_{Strn4\text{-}SCKO} = 0.4678$, $p_{Strn1/3\text{-}dSCKO} < 0.0001$, $p_{Strn1/4\text{-}dSCKO} > 0.9999$, and $p_{Strn3/4\text{-}dSCKO} < 0.0001$). Fiber density ($F$ (5, 35) model = 34.94; $p < 0.0001$; F (1, 35) WT versus KO = 71.50, $p < 0.0001$; $p_{Strn1\text{-}SCKO} > 0.9999$, $p_{Strn3\text{-}SCKO} > 0.9999$, $p_{Strn4\text{-}SCKO} > 0.9999$, $p_{Strn1/3\text{-}dSCKO} < 0.0001$, $p_{Strn1/4\text{-}dSCKO} > 0.9999$, and $p_{Strn3/4\text{-}dSCKO} < 0.0001$). Nerve area ($F$ (5, 35) model = 4.602; $p = 0.0025$; F (1, 35) WT versus KO = 11.41, $p = 0.0018$; $p_{Strn1\text{-}SCKO} > 0.9999$, $p_{Strn3\text{-}SCKO} > 0.9999$, $p_{Strn4\text{-}SCKO} > 0.9999$, $p_{Strn1/3\text{-}dSCKO} = 0.0001$, $p_{Strn1/4\text{-}dSCKO} > 0.9999$, and $p_{Strn3/4\text{-}dSCKO} = 0.0117$). Error bars indicate SEM. *$p < 0.05$, ***$p < 0.001$, and ****$p < 0.0001$.

STRN1 and STRN3 are downstream of Rac1 activity. Second, we looked at the mRNA, total protein levels, and phosphorylation of MST1, MST2, YAP, and TAZ in mice with SC-specific deletion of *Rac1* (Rac1^{SCKO}) mice. Overall, our data show that the absence of Rac1 in SCs also leads to a global increase in the phosphorylation of Hippo pathway members (Figures S9C–S9E). We also found that MST1/2 total protein levels were reduced in Rac1^{SCKO} peripheral nerves, which correlated with reduced *Mst2* mRNA at P5 (Figures S9A and S9B). However, unlike Strn1/3^{dSCKO} mice, we did not find altered levels of total YAP or TAZ (Figures S9C–S9E). Thus, these data suggest that the loss of Rac1 in SCs causes Hippo pathway overactivation at the level of MST1 and MST2, with subsequent phosphorylation and inhibition of YAP and TAZ.

STRN1, STRN3, and Rac1 regulate SC laminin receptor expression and differentiation

Multiple studies have found that SC expression of several laminin receptors is dependent on YAP- and TAZ-mediated transcription.[17,19] In addition, YAP- and TAZ-mediated transcription is necessary for SC expression of the master transcription factor *Egr2*.[17,19,20] We, therefore, hypothesized that the peripheral nerve developmental defects observed in Strn1/3^{dSCKO} mice may be associated with a reduction in the YAP/TAZ-dependent

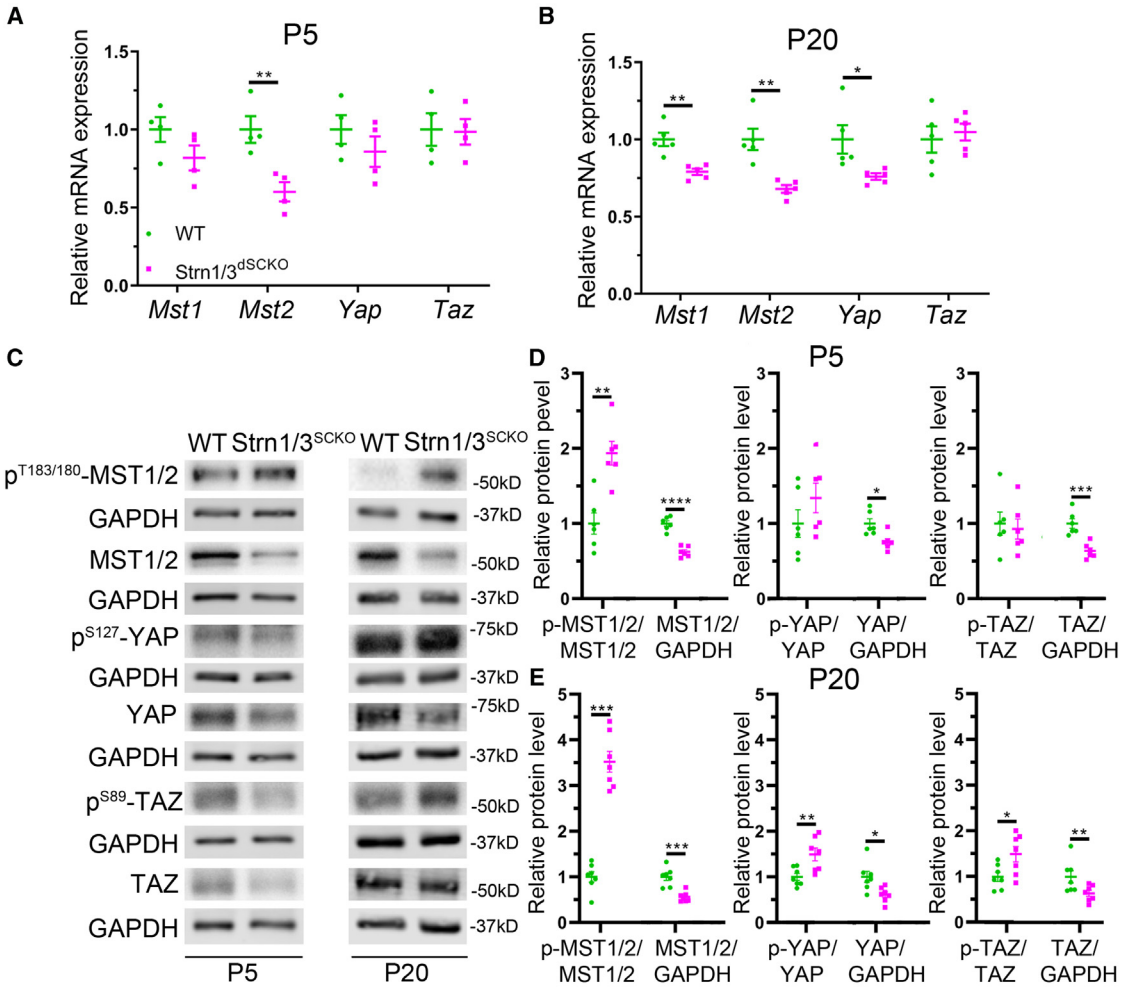

Figure 5. Strn1/3 ablation in SCs results in Hippo pathway dysregulation

(A and B) mRNA expression of *Mst1*, *Mst2*, *Yap*, and *Taz* from pooled sciatic nerves and brachial plexuses of WT and Strn1/3^{dSCKO} mice at P5 and P20. *Mst2* mRNA level is decreased at P5 and P20, while *Mst1* and *Yap* mRNA levels are decreased at P20 in peripheral nerves of Strn1/3^{SCKO} mice. $N = 4–5$ samples per genotype. P5 samples were pooled from 3–6 animals each. Unpaired two-tailed t test. P5 (*Mst1* [$t = 1.625$, df = 6, $p = 0.1553$], *Mst2* [$t = 3.789$, df = 6, $p = 0.0091$], *Yap* [$t = 1.061$, df = 6, $p = 0.3296$], and *Taz* [$t = 0.1119$, df = 6, $p = 0.9145$]). P20 (*Mst1* [$t = 4.363$, df = 8, $p = 0.0024$], *Mst2* [$t = 4.368$, df = 8, $p = 0.0024$], *Yap* [$t = 2.562$, df = 8, $p = 0.0335$], and *Taz* [$t = 0.4670$, df = 8, $p = 0.6529$]).

(C) Representative western blots of several Hippo pathways effectors from pooled sciatic nerves and brachial plexuses of WT and Strn1/3^{dSCKO} mice at P5 and P20.

(D and E) Densitometry analysis shows a reduction in total MST1/2, YAP, and TAZ at P5 and P20, an increase in p-MST1/2 at P5, and an increase in p-MST1/2, p-YAP, and p-TAZ at P20 in peripheral nerves of Strn1/3^{dSCKO} mice. $n = 6–7$ samples per genotype. P5 samples were pooled from 3–6 animals each. Unpaired two-tailed t test. P5 (p-MST1/2 [$t = 4.431$, df = 10, $p = 0.0013$], MST1/2 [$t = 8.115$, df = 10, $p < 0.0001$], p-YAP [$t = 1.267$, df = 10, $p = 0.2340$], YAP [$t = 3.119$, df = 10, $p = 0.0109$], p-TAZ [$t = 0.3535$, df = 10, $p = 0.7311$], and TAZ [$t = 4.803$, df = 10, $p = 0.0007$]). P20 (p-MST1/2 [$t = 6.906$, df = 12, $p < 0.0001$], MST1/2 [$t = 5.089$, df = 12, $p = 0.0003$], p-YAP [$t = 3.089$, df = 12, $p = 0.0094$], YAP [$t = 2.890$, df = 12, $p = 0.0136$], p-TAZ [$t = 2.534$, df = 12, $p = 0.0267$], and TAZ [$t = 2.378$, df = 12, $p = 0.0349$]). Error bars indicate SEM.

*$p < 0.05$, **$p < 0.01$, ***$p < 0.001$, ****$p < 0.0001$.

expression of laminin receptors and *Egr2*, with a subsequent retention of *Pou3f1* expression and failure of differentiation from immature/promyelinating (POU3F1+) to myelinating (EGR2+) SCs.[34–40]

Gene expression analyses revealed several laminin receptors (*Itga6*, *Itgb1*, and *Itgb4*) that were transcriptionally downregulated in Strn1/3^{dSCKO} peripheral nerves at P5, with the downregulation of *Itga6* persisting at P20 (Figures 7A and 7B). At the protein level, we found reduced integrin α6, integrin β1, and integrin β4 subunits, as well as β-dystroglycan, at both P5 and P20 in peripheral nerves of Strn1/3^{dSCKO} mice, suggesting an early and persistent defect in laminin receptor expression (Figures 7C–7E and S10). The absence of STRN1 and STRN3 also led to an increase in *Pou3f1* mRNA and protein levels and a decrease in *Egr2* mRNA and protein levels (Figure 7). Because we previously demonstrated that defects in radial sorting in YAP and TAZ mutants were associated with defects in SC proliferation,[17] we assessed the number of proliferative SCs. While we

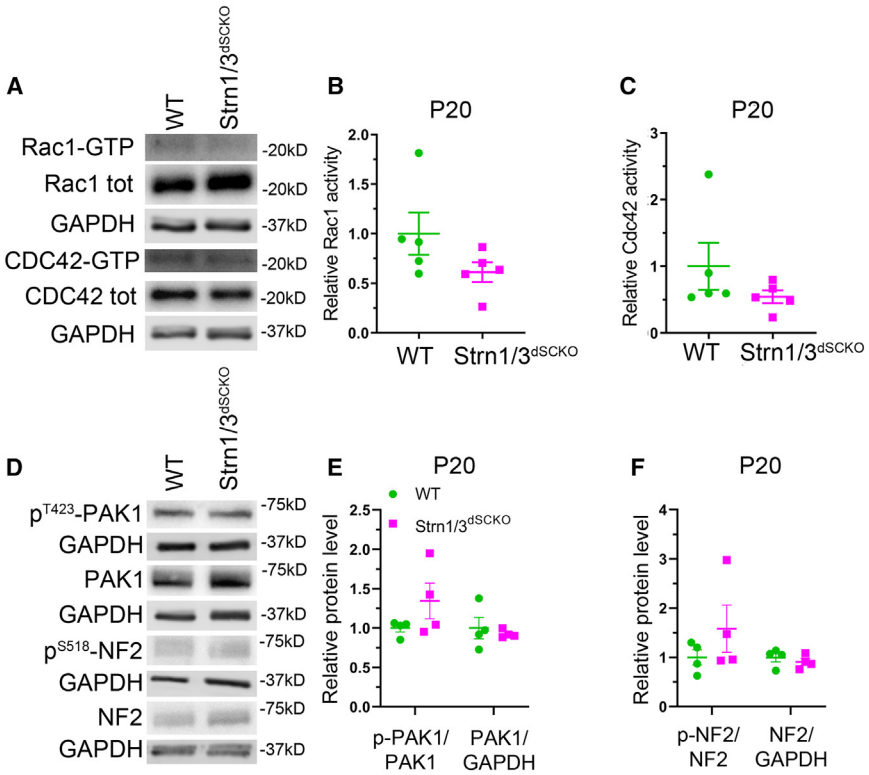

Figure 6. Ablation of Strn1 and Strn3 in SCs does not alter Rac1 activity

(A) Representative western blots of Rac1 and CDC42 active (GTP) and total (tot) forms from pooled P20 sciatic nerves and brachial plexuses of WT and Strn1/3^{dSCKO} mice.

(B and C) Densitometry analysis shows no significant change in Rac1 or CDC42 activity in peripheral nerves of Strn1/3^{dSCKO} mice at P20. $n = 5$ samples per genotype. Samples were pooled from 3–5 animals each. Unpaired two-tailed t test. Rac1 activity ($t = 1.649$, df = 8, $p = 0.1379$) and CDC42 activity ($t = 1.257$, df = 8, $p = 0.2443$).

(D) Representative western blots of PAK1 and NF2 phosphorylated and tot forms from P20 sciatic nerves and brachial plexuses of WT and Strn1/3^{dSCKO} mice.

(E and F) Densitometry analysis shows no significant change in phosphorylation or tot levels of the Rac1/CDC42 effectors PAK1 or NF2 in peripheral nerves of Strn1/3^{dSCKO} mice at P20. $n = 4$ animals per genotype. Unpaired two-tailed t test. p-PAK1 ($t = 1.484$, df = 6, $p = 0.1884$), PAK1 ($t = 0.5307$, df = 6, $p = 0.6147$), p-NF2 ($t = 1.160$, df = 6, $p = 0.2900$), and NF2 ($t = 0.7988$, df = 6, $p = 0.4548$). Error bars indicate SEM.

did not observe a significant reduction in SC number or SC proliferation at P5 (Figure 7F), we found that at P20, the number of proliferative SCs was increased in Strn1/3^{dSCKO} nerves, correlating with increased levels of POU3F1, a marker for immature and promyelinating SCs, stages during which SCs normally undergo greater proliferation (Figure 7G). These findings support our observations in Strn1/3^{dSCKO} sciatic nerves (Figure 4) of a severe radial sorting delay with an associated temporal shift in SC proliferation, excess numbers of immature/promyelinating SCs (POU3F1+), and a reduced number of mature, myelinating SCs (EGR2+).

Finally, we found that Rac1^{SCKO} peripheral nerves recapitulate many of the phenotypes observed in Strn1/3^{dSCKO} mice on laminin receptor, *Pou3f1*, and *Egr2* mRNA and protein levels (Figure S11). These data suggest that the absence of Rac1 in SCs is associated with a downregulation of laminin receptors and EGR2 with a concomitant upregulation of POU3F1. Altogether, our results strongly indicate that Rac1, STRN1, and STRN3 modulate developmentally crucial gene expression in SCs through the Hippo pathway, YAP, and TAZ.

DISCUSSION

In this study, we identified a previously unknown interaction between Rac1 and two STRIPAK complex members, STRN3 and MOB4. We found that members of the striatin family of proteins are essential in SCs for axonal radial sorting and SC differentiation. Additionally, the loss of Rac1 or STRN1/3 resulted in the dysregulation of Hippo pathway signaling, YAP/TAZ activity, laminin receptor expression, and expression of the master transcription factor EGR2. Furthermore, we found that the loss of STRN1 and STRN3 resulted in a global breakdown in the abundance of other STRIPAK complex members.

Signals from the SC-derived basal lamina, transmitted via laminin receptors, are required for SC proliferation, survival, differentiation, apical-basal polarity, radial sorting, initiation of myelination, radial and longitudinal growth of the myelin sheath, and nodal clustering of voltage-gated sodium channels.[1–12] Among the signals initiated upon receptor-ECM ligand engagement is Rho GTPase activity. Rac1 and a closely related Rho GTPase, CDC42, have previously been shown to be required for SCs to radially sort and myelinate axons.[6,13–15] Rac1 has also been shown to be required for the early SC response to peripheral nerve injury, an organized process by which SCs initiate myelin fragmentation and digestion.[41] The expression of dominant-negative NF2, a downstream Rac1/CDC42 effector, partially rescues the developmental myelination defect in both Rac1 and CDC42 mutant mice but rescues the radial sorting defect in only CDC42 mutant mice.[14,15] Our understanding of how, precisely, NF2 mediates this partial rescue, the difference between Rac1 and CDC42 mutant mice, and the additional mechanisms mediating radial sorting and myelination defects in these models remains limited.

Previous studies have found conflicting reports about the influence of Rac1 on Hippo pathway signaling and YAP/TAZ activity in a variety of cell types *in vitro*.[42–45] Additionally, multiple groups have reported mechanisms by which NF2, a Rac1 effector, influences STRIPAK-independent and STRIPAK-dependent regulation of the Hippo pathway.[26,27,43,46,47] One STRIPAK-independent

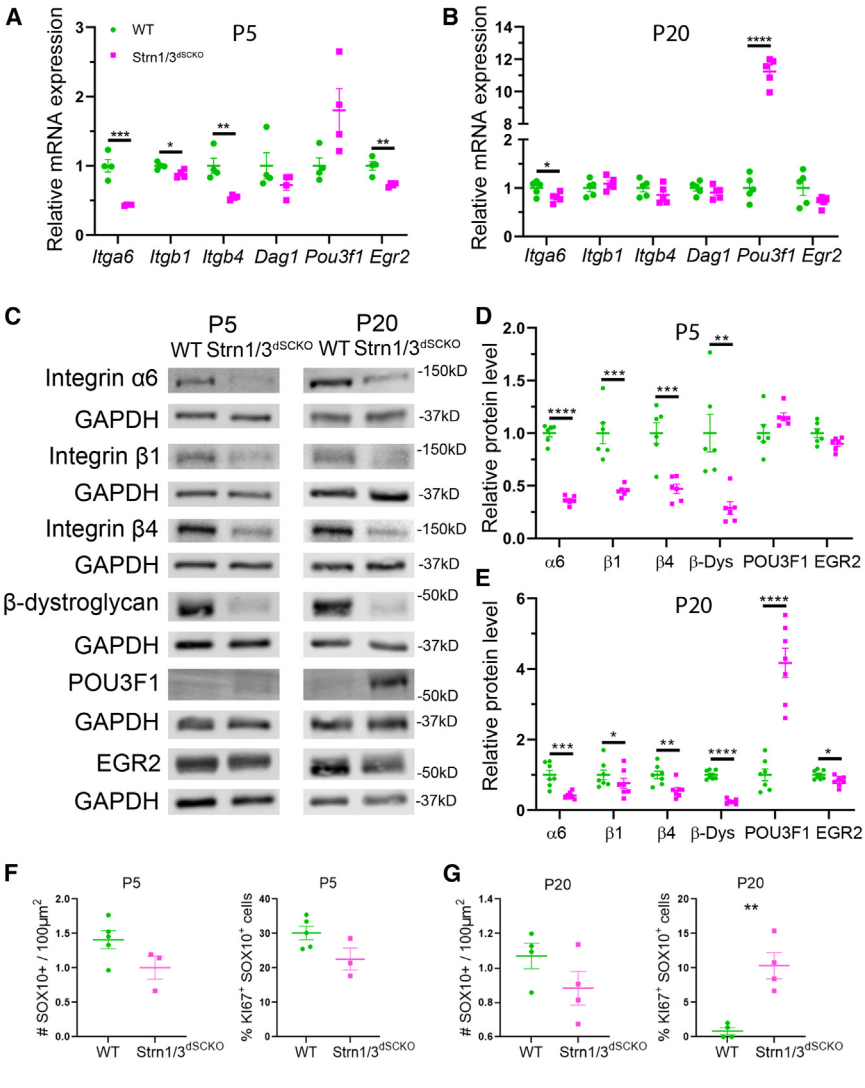

Figure 7. Strn1 and Strn3 ablation in SCs results in dysregulated mRNA and protein expression of laminin receptors and SC transcriptional regulators

(A and B) mRNA expression of several laminin receptors (encoding for integrin subunits α6 [*Itga6*], β1 [*Itgb1*], and β4 [*Itgb4*] and β-dystroglycan [*Dag1*]) and SC development transcriptional regulators (*Pou3f1* and *Egr2*) from pooled sciatic nerves and brachial plexuses of WT and Strn1/3^{dSCKO} mice at P5 and P20. *Itgb1*, *Itgtb4*, and *Egr2* mRNA levels are decreased at P5, *Itga6* mRNA level is decreased at P5 and P20, and *Pou3f1* mRNA level is increased at P20 in peripheral nerves of Strn1/3^{dSCKO} mice. $n = 4–5$ samples per genotype. P5 samples were pooled from 3–6 animals each. Unpaired two-tailed t test. P5 (*Itga6* [$t = 6.236$, df = 6, $p = 0.0008$], *Itgb1* [$t = 3.094$, df = 6, $p = 0.0213$], *Itgb4* [$t = 4.102$, df = 6, $p = 0.0063$], *Dag1* [$t = 1.341$, df = 6, $p = 0.2284$], *Pou3f1* [$t = 2.380$, df = 6, $p = 0.0548$], and *Egr2* [$t = 4.288$, df = 6, $p = 0.0052$]). P20 (*Itga6* [$t = 2.487$, df = 8, $p = 0.0377$], *Itgb1* [$t = 0.9136$, df = 8, $p = 0.3876$], *Itgb4* [$t = 1.254$, df = 8, $p = 0.2451$], *Dag1* [$t = 1.103$, df = 8, $p = 0.3020$], *Pou3f1* [$t = 25.75$, df = 8, $p < 0.0001$], and *Egr2* [$t = 1.722$, df = 8, $p = 0.1233$]).

(C) Representative western blots of several laminin receptors and SC development transcriptional regulators from pooled sciatic nerves and brachial plexuses of WT and Strn1/3^{dSCKO} mice at P5 and P20.

(D and E) Densitometry analysis shows a reduction in integrin α6, β1, and β4 subunits and β-dystroglycan at P5 and P20, an increase in POU3F1 at P20, and a reduction in EGR2 at P20 in peripheral nerves of Strn1/3^{dSCKO} mice. $n = 6–7$ samples per genotype. P5 samples were pooled from 3–6 animals each. Unpaired two-tailed t test. P5 (integrin α6 [$t = 16.27$, df = 10, $p < 0.0001$], integrin β1 [$t = 5.328$, df = 10, $p = 0.0003$], integrin β4 [$t = 4.826$, df = 10, $p = 0.0007$], β-dystroglycan [$t = 3.777$, df = 10, $p = 0.0036$], POU3F1 [$t = 1.717$, df = 10, $p = 0.1168$], and EGR2 [$t = 2.053$, df = 10, $p = 0.0671$]). P20 (integrin α6 [$t = 4.446$, df = 12, $p = 0.0008$], integrin β1 [$t = 2.994$, df = 12, $p = 0.0112$], integrin β4 [$t = 3.277$, df = 12, $p = 0.0066$], β-dystroglycan [$t = 13.65$, df = 12, $p < 0.0001$], POU3F1 [$t = 7.137$, df = 12, $p < 0.0001$], and EGR2 [$t = 2.443$, df = 12, $p = 0.0310$]).

(F and G) Quantification of the total number of SCs (SOX10+) and proliferative SCs (SOX10+ KI67+) at P5 and P20 shows an increase in SC proliferation at P20 in peripheral nerves of Strn1/3^{dSCKO} mice but no difference in numbers of SCs at either age. $n = 3–5$ samples per genotype. Unpaired two-tailed t test. P5 (SOX10+ [$t = 1.908$, df = 6, $p = 0.1051$] and KI67+SOX10+ [$t = 2.179$, df = 6, $p = 0.0722$]). P20 (SOX10+ [$t = 1.532$, df = 6, $p = 0.1764$] and KI67+SOX10+ [$t = 4.847$, df = 6, $p = 0.0029$]).

Error bars indicate SEM. *$p < 0.05$, **$p < 0.01$, ***$p < 0.001$, and ****$p < 0.0001$.

mechanism suggests that NF2 directly interacts with AMOT, a YAP effector and binding partner, thereby acting as a bridge to promote LATS1/2-mediated phosphorylation of YAP.[43] A STRIPAK-dependent mechanism suggests that SAV1, an MST1/2 adaptor protein, preserves MST1/2 activity by antagonizing STRIPAK/PP2A-mediated dephosphorylation of p-MST1/2 (Thr183/180).[26] Deleting the N-terminal portion of SAV1, which includes its NF2 binding domain, reduced its ability to preserve MST1/2 activity, suggesting that NF2 may influence SAV1-mediated antagonism of STRIPAK. Another STRIPAK-dependent mechanism suggests that NF2 interacts with STRIPAK via the STRIP1 STRIPAK adaptor protein to prevent the association of the PP2A phosphatase with STRIPAK complexes.[27] Of note, loss of NF2 in SCs has been demonstrated to result in defects in axonal regeneration and remyelination following peripheral nerve injury, which is rescued by the co-deletion of *Yap* in SCs.[48] However, this result contrasts somewhat with more recent studies that demonstrate a defect in remyelination following peripheral nerve injury in mice lacking both YAP and TAZ in SCs.[49,50] Our results indicate that the ablation of *Rac1* in SCs *in vivo* results in Hippo pathway activation and YAP/TAZ inhibition with a subsequent loss of YAP/TAZ-mediated laminin receptor and transcription factor expression.[17,19,20] We propose that this overactive Hippo signaling and its downstream effects are responsible for a portion of both the NF2-dependent and NF2-independent peripheral nerve developmental defects in Rac1^{SCKO}

and possibly CDC42^{SCKO} mice. We believe that a similar mechanism is responsible for the more severe phenotype observed in Strn1/3^{dSCKO} mice. Further studies could confirm the specific roles of Hippo pathway signaling in these models by targeting the upstream Hippo pathway pharmacologically, such as with the MST1/2 inhibitor XMU-MP-1, or with conditional mutagenesis approaches.[51–53]

Importantly, aside from its function in modulating Hippo pathway signaling, the STRIPAK complex has been implicated in many other cellular functions, as has been extensively reviewed elsewhere.[54–56] For example, there is evidence for a direct role of STRIPAK in TORC2, JNK, p38 MAPK, and RhoA signaling and in processes such as synaptic terminal formation, mitophagy, and autophagosome fusion.[57–59] Thus, it is possible that the phenotype observed in the Strn1/3^{dSCKO} model is caused by Hippo-independent mechanisms. First, in the Strn1/3^{dSCKO} model, there is a severe disruption in the expression of various laminin receptor subunits, which we believe may alone be sufficient to elicit the extreme morphological phenotype observed.[6] Second, it is plausible that there are also direct, STRIPAK-mediated effects on the actin cytoskeleton. It has already been demonstrated that Rac1 is essential for lamellipodia formation, process elongation, and injury-induced actin polymerization.[6,13,41] In addition, Rac1 activity has previously been demonstrated to have multiple pronounced effects on the actin dynamics of peripheral ensheathing glia of *Drosophila melanogaster*.[60] Of note, these mechanisms are not mutually exclusive to the previously published literature. Additionally, modulation of the actin cytoskeleton is also known to regulate YAP and TAZ in a Hippo-independent manner.[61,62]

Our finding of a direct interaction between Rac1 and STRN3/MOB4 suggests a mechanism for linking Rac1 activity and Hippo pathway signaling. This is an intriguing possibility, given the diverse roles of YAP/TAZ in SCs and that Rac1 and various STRIPAK complex subunits are druggable targets. The loss of either Rac1 or STRN1/3 in SCs results in MST1/2 overactivation and YAP/TAZ inhibition by phosphorylation. However, further work is required to prove a STRIPAK-dependent mechanism of Hippo pathway regulation by Rac1. Future studies could seek to clarify the purpose of these Rac1-STRIPAK interactions, perhaps by transgenic depletion of STRN3, MOB4, or PP2A, pharmacologic modulation of PP2A activity with drugs like okadaic acid, disruption of the Rac1-STRN3 or Rac1-MOB4 interactions, or disruption of the STRN3-PP2A interaction necessary for STRIPAK-mediated inhibition of the Hippo pathway. Exciting technologies for the latter, such as a STRN3-derived Hippo-activating peptide (SHAP) and improved heterocyclic PP2A activators (iHAPs), have recently been described.[32,63]

Interestingly, we found reduced total levels of the MST1/2 kinases following the ablation of Rac1 or STRN1/3, and this appeared to be partially mediated by transcriptional repression. To the best of our knowledge, the downregulation of total MST1/2 as a regulatory mechanism has not been previously described in any cell type. We propose that this reduction in total MST1/2 could represent a previously undescribed Hippo pathway regulatory feedback loop. In the context of overactive MST1/2 kinase activity, partial suppression of this aberrant signaling may be achieved via a reduction in total protein levels. While our results indicate that this effect is partly transcriptionally mediated, additional investigations will be required to determine how this transcriptional response is initiated and what other mechanisms may be involved. Developments in targeting MST1/2 are exciting prospects, given the broad interest in modifying Hippo pathway signaling in fields as diverse as developmental disorders, regenerative medicine, and oncology.[64]

To the best of our knowledge, the reduction in protein levels of various STRIPAK complex subunits (STRN4, MOB4, STRIP1, and CCM3) following the loss of the central striatin scaffolding proteins has not been previously described. We had anticipated potential protein instability of STRIPAK subunits following *Strn1/3* deletion; however, the additional reduction in STRN4 levels was surprising due to its upregulation following single *Strn3* ablation in SCs. Given the markedly reduced phenotypic severity of STRN1/4^{dSCKO} mice compared to STRN1/3^{dSCKO} or STRN3/4^{dSCKO} mice, our results indicate that STRN3 is the only striatin protein sufficient to perform the majority of striatin family protein functions during SC development alone. Altogether, these results suggest that STRN3 is particularly important for the stability of STRIPAK complexes and for STRIPAK functions. The role of STRN3 in STRIPAK complex integrity may be of particular interest to groups studying the Hippo pathway in various disease contexts, given the involvement of STRIPAK adaptor proteins such as MOB4, STRIP1, and CCM3 in regulating the Hippo pathway in diseases such as pancreatic cancer, gastric cancer, hepatocellular carcinoma, and breast cancer.[27,65–67] Recent studies have also found STRN3 to be notable among the striatins, such as in its ability to form asymmetric homotetramers with a single catalytic STRIPAK core.[29] Additionally, while all three striatin proteins and their inhibitory effect on the Hippo pathway have been correlated with human cancers, STRN3 is cited in a particularly wide array of human cancer subtypes, including various immortalized cancer cell lines (hepatocellular carcinoma, prostatic adenocarcinoma, and medulloblastoma); patient-derived primary cultures and biopsy specimens (gastric cancer, hepatocellular carcinoma, cribriform adenocarcinoma of the salivary gland, and breast cancer); and estrogen receptor (ER)-dependent clinical outcomes of patients with breast cancer (possibly due to inhibition of ERα by STRN3).[32,68–73] We believe that our findings and others make STRN3 a useful starting candidate in future investigations of STRIPAK biology.

It is inherently difficult to parse out radial sorting and myelination defects, as both developmental processes occur in a similar time window. Animals with radial sorting defects can have concomitant myelination defects, such as excess numbers of promyelinating SCs, abnormal myelin features, and/or hypomyelination.[6,17] However, mutants with radial sorting defects can also present without myelination defects, such as in *Lama2*$^{-/-}$ mice.[74] While STRN3^{SCKO} and STRN1/3^{dSCKO} mice present with defects in myelin formation, supporting that striatins are required for the myelination step of SC development, the principal role of striatins appears to be in facilitating radial sorting.

In conclusion, our study reveals that striatin proteins are critical for SC radial sorting and subsequent myelination and that loss of STRN1/3 or Rac1 results in a profound deficit in laminin receptor expression and SC differentiation, possibly via dysregulation of Hippo pathway signaling. The influence of the Hippo pathway

and YAP/TAZ on regulating peripheral neuropathy disease-associated gene expression, tumor progression in cancers such as malignant peripheral nerve sheath tumors, and remyelination with functional recovery following peripheral nerve injury is gaining increased attention.[16,17,19,20,48–50,53,75–78] Our study adds to the growing body of knowledge about the modulation of the Hippo pathway and YAP/TAZ by identifying previously undescribed Hippo/YAP/TAZ regulatory machinery in SCs.[79] Namely, we have demonstrated the marked dysregulation of Hippo signaling and YAP/TAZ activity following *Rac1* or *Strn1/3* ablation in SCs. Additionally, our work proposes multiple paradigms for modifying Hippo pathway signaling in SCs, such as by targeting Rac1-STRN3/MOB4 interactions, MST1/2 protein abundance, or STRIPAK complex integrity. Rac1-STRN3/MOB4 interactions and the loss of STRIPAK complex integrity following deletion of *Strn1/3* also uncover previously undescribed aspects of basic STRIPAK biology. We posit that further investigation of STRIPAK complexes will establish if they regulate ECM receptor expression or cellular differentiation in other cell types and lead to a better understanding of their influence in modulating a variety of additional cellular functions in SCs. This research could spur the development of STRIPAK-targeting therapeutic approaches with applications in diverse fields such as peripheral nerve development, peripheral neuropathies, peripheral nerve tumors, and peripheral nerve regeneration.

Limitations of the study

In our investigations of RAC1 interactions with STRN3 and MOB4, we show conflicting evidence of a binding preference for active, GTP-bound RAC1. We believe that other members of this complex, such as additional STRIPAK proteins, may be responsible for modifying this interaction. However, we did not pursue this hypothesis, and it remains unclear how this interaction may be modified. Additionally, while we show that the loss of STRN1/3 does not influence RAC1 activity, we did not attempt further exploration of the purpose of the interaction of RAC1 with STRN3 and MOB4. Therefore, the reason for this interaction and any cross-regulation or signaling it influences remains uncertain.

In our analyses of various protein and mRNA levels in the Strn1/3^{dSCKO} mice, we normalized to the housekeeping gene GAPDH, which is expressed by both axons and cells of the SC lineage (Sox10+ cells). While our data show no significant difference in Sox10+ cells at P5 or P20, there does appear to be a small trend (p = 0.1051) toward reduced Sox10+ cells at P5, which may artificially contribute to some of the more modest reductions observed in protein or mRNA levels. Further validation would be helpful to confirm an SC-specific reduction in targets with more modest changes to protein and mRNA levels following loss of STRN1/3.

RESOURCE AVAILABILITY

Lead contact

Requests for further information, resources, and reagents should be directed to and will be fulfilled by the lead contact, Yannick Poitelon (poitely@amc.edu)

Materials availability

This study did not generate unique reagents.

Data and code availability

- All data reported in this paper will be shared by the lead contact upon request.
- This paper does not report original code.
- Any additional information required to reanalyze the data reported in this paper is available from the lead contact upon request.

ACKNOWLEDGMENTS

This work was funded by NIH NINDS R01 NS045630 (to M.L.F.), F30 NS118774 (to M.R.W.), R01 NS134493 (to S.B.), and R01 NS110627 (to Y.P.). We thank Gustavo Della-Flora Nunez and Emma R. Wilson for their technical assistance.

AUTHOR CONTRIBUTIONS

M.R.W. and M.L.F. designed the research. M.R.W. carried out the majority of the experiments. D.S. quantified myelinated fibers and nerve cross-sectional areas in semithin section images. S.P. and S.B. quantified the P60 g-ratio in semithin section images. J.F. and Y.P. quantified SC density and proliferation. M.L.F. quantified myelin abnormalities and amyelinated fibers in electron microscopy images. E.H. processed tissue for morphological analyses. M. Pellegatta, C.B., M. Palmisano, and S.F. performed the initial GST pull-down screen for Rac1 interactors. M.S. and F.E.P. performed mass spectroscopy. M.R.W., M.L.F., and Y.P. analyzed the data. M.R.W. and Y.P. wrote the manuscript. F.S. critically reviewed the manuscript.

DECLARATION OF INTERESTS

The authors declare no competing interests.

STAR★METHODS

Detailed methods are provided in the online version of this paper and include the following:

- KEY RESOURCES TABLE
- EXPERIMENTAL MODEL AND STUDY PARTICIPANT DETAILS
  - Animal models
  - Cell culture
- METHOD DETAILS
  - Rac1 activity assay
  - Rac1 pull-down assay
  - Co-immunoprecipitation (coIP)
  - Proximity ligation assay
  - Dot blot
  - Genotyping
  - Morphological assessment
  - RNA extraction and RT-qPCR analysis
  - Western blot
  - Immunofluorescence
- QUANTIFICATION AND STATISTICAL ANALYSIS

SUPPLEMENTAL INFORMATION

Supplemental information can be found online at https://doi.org/10.1016/j.celrep.2025.115401.

Received: May 3, 2024
Revised: January 19, 2025
Accepted: February 14, 2025

REFERENCES

1. Berti, C., Bartesaghi, L., Ghidinelli, M., Zambroni, D., Figlia, G., Chen, Z.L., Quattrini, A., Wrabetz, L., and Feltri, M.L. (2011). Non-redundant function

of dystroglycan and β1 integrins in radial sorting of axons. Development *138*, 4025–4037.

2. Court, F.A., Hewitt, J.E., Davies, K., Patton, B.L., Uncini, A., Wrabetz, L., and Feltri, M.L. (2009). A laminin-2, dystroglycan, utrophin axis is required for compartmentalization and elongation of myelin segments. J. Neurosci. *29*, 3908–3919.
3. Feltri, M.L., Graus Porta, D., Previtali, S.C., Nodari, A., Migliavacca, B., Cassetti, A., Littlewood-Evans, A., Reichardt, L.F., Messing, A., Quattrini, A., et al. (2002). Conditional disruption of beta 1 integrin in Schwann cells impedes interactions with axons. J. Cell Biol. *156*, 199–209.
4. Feltri, M.L., Poitelon, Y., and Previtali, S.C. (2016). How Schwann Cells Sort Axons: New Concepts. Neuroscientist *22*, 252–265.
5. Nodari, A., Previtali, S.C., Dati, G., Occhi, S., Court, F.A., Colombelli, C., Zambroni, D., Dina, G., Del Carro, U., Campbell, K.P., et al. (2008). Alpha6-beta4 integrin and dystroglycan cooperate to stabilize the myelin sheath. J. Neurosci. *28*, 6714–6719.
6. Nodari, A., Zambroni, D., Quattrini, A., Court, F.A., D'Urso, A., Recchia, A., Tybulewicz, V.L.J., Wrabetz, L., and Feltri, M.L. (2007). Beta1 integrin activates Rac1 in Schwann cells to generate radial lamellae during axonal sorting and myelination. J. Cell Biol. *177*, 1063–1075.
7. Occhi, S., Zambroni, D., Del Carro, U., Amadio, S., Sirkowski, E.E., Scherer, S.S., Campbell, K.P., Moore, S.A., Chen, Z.L., Strickland, S., et al. (2005). Both laminin and Schwann cell dystroglycan are necessary for proper clustering of sodium channels at nodes of Ranvier. J. Neurosci. *25*, 9418–9427.
8. Pellegatta, M., De Arcangelis, A., D'Urso, A., Nodari, A., Zambroni, D., Ghidinelli, M., Matafora, V., Williamson, C., Georges-Labouesse, E., Kreidberg, J., et al. (2013). α6β1 and α7β1 integrins are required in Schwann cells to sort axons. J. Neurosci. *33*, 17995–18007.
9. Previtali, S.C., Dina, G., Nodari, A., Fasolini, M., Wrabetz, L., Mayer, U., Feltri, M.L., and Quattrini, A. (2003a). Schwann cells synthesize alpha7-beta1 integrin which is dispensable for peripheral nerve development and myelination. Mol. Cell. Neurosci. *23*, 210–218.
10. Previtali, S.C., Nodari, A., Taveggia, C., Pardini, C., Dina, G., Villa, A., Wrabetz, L., Quattrini, A., and Feltri, M.L. (2003b). Expression of laminin receptors in Schwann cell differentiation: evidence for distinct roles. J. Neurosci. *23*, 5520–5530.
11. Saito, F., Moore, S.A., Barresi, R., Henry, M.D., Messing, A., Ross-Barta, S.E., Cohn, R.D., Williamson, R.A., Sluka, K.A., Sherman, D.L., et al. (2003). Unique role of dystroglycan in peripheral nerve myelination, nodal structure, and sodium channel stabilization. Neuron *38*, 747–758.
12. Yu, W.M., Feltri, M.L., Wrabetz, L., Strickland, S., and Chen, Z.L. (2005). Schwann cell-specific ablation of laminin gamma1 causes apoptosis and prevents proliferation. J. Neurosci. *25*, 4463–4472.
13. Benninger, Y., Thurnherr, T., Pereira, J.A., Krause, S., Wu, X., Chrostek-Grashoff, A., Herzog, D., Nave, K.A., Franklin, R.J.M., Meijer, D., et al. (2007). Essential and distinct roles for cdc42 and rac1 in the regulation of Schwann cell biology during peripheral nervous system development. J. Cell Biol. *177*, 1051–1061.
14. Guo, L., Moon, C., Niehaus, K., Zheng, Y., and Ratner, N. (2012). Rac1 controls Schwann cell myelination through cAMP and NF2/merlin. J. Neurosci. *32*, 17251–17261.
15. Guo, L., Moon, C., Zheng, Y., and Ratner, N. (2013). Cdc42 regulates Schwann cell radial sorting and myelin sheath folding through NF2/merlin-dependent and independent signaling. Glia *61*, 1906–1921.
16. Feltri, M.L., Weaver, M.R., Belin, S., and Poitelon, Y. (2021). The Hippo pathway: Horizons for innovative treatments of peripheral nerve diseases. J. Peripher. Nerv. Syst. *26*, 4–16.
17. Poitelon, Y., Lopez-Anido, C., Catignas, K., Berti, C., Palmisano, M., Williamson, C., Ameroso, D., Abiko, K., Hwang, Y., Gregorieff, A., et al. (2016). YAP and TAZ control peripheral myelination and the expression of laminin receptors in Schwann cells. Nat. Neurosci. *19*, 879–887.
18. Belin, S., Herron, J., VerPlank, J.J.S., Park, Y., Feltri, L.M., and Poitelon, Y. (2019). Corrigendum: YAP and TAZ Regulate *Cc2d1b* and *Pur* β in Schwann Cells. Front. Mol. Neurosci. *12*, 256.
19. Deng, Y., Wu, L.M.N., Bai, S., Zhao, C., Wang, H., Wang, J., Xu, L., Sakabe, M., Zhou, W., Xin, M., and Lu, Q.R. (2017). A reciprocal regulatory loop between TAZ/YAP and G-protein Gαs regulates Schwann cell proliferation and myelination. Nat. Commun. *8*, 15161.
20. Grove, M., Kim, H., Santerre, M., Krupka, A.J., Han, S.B., Zhai, J., Cho, J.Y., Park, R., Harris, M., Kim, S., et al. (2017). YAP/TAZ initiate and maintain Schwann cell myelination. Elife *6*, e20982.
21. Hong, J., Kirkland, J.M., Acheta, J., Marziali, L.N., Beck, B., Jeanette, H., Bhatia, U., Davis, G., Herron, J., Roué, C., et al. (2024). YAP and TAZ regulate remyelination in the central nervous system. Glia *72*, 156–166.
22. Feltri, M.L., D'Antonio, M., Previtali, S., Fasolini, M., Messing, A., and Wrabetz, L. (1999). P0-Cre transgenic mice for inactivation of adhesion molecules in Schwann cells. Ann. N. Y. Acad. Sci. *883*, 116–123.
23. Castets, F., Bartoli, M., Barnier, J.V., Baillat, G., Salin, P., Moqrich, A., Bourgeois, J.P., Denizot, F., Rougon, G., Calothy, G., and Monneron, A. (1996). A novel calmodulin-binding protein, belonging to the WD-repeat family, is localized in dendrites of a subset of CNS neurons. J. Cell Biol. *134*, 1051–1062.
24. Castets, F., Rakitina, T., Gaillard, S., Moqrich, A., Mattei, M.G., and Monneron, A. (2000). Zinedin, SG2NA, and striatin are calmodulin-binding, WD repeat proteins principally expressed in the brain. J. Biol. Chem. *275*, 19970–19977.
25. Goudreault, M., D'Ambrosio, L.M., Kean, M.J., Mullin, M.J., Larsen, B.G., Sanchez, A., Chaudhry, S., Chen, G.I., Sicheri, F., Nesvizhskii, A.I., et al. (2009). A PP2A phosphatase high density interaction network identifies a novel striatin-interacting phosphatase and kinase complex linked to the cerebral cavernous malformation 3 (CCM3) protein. Mol. Cell. Proteomics *8*, 157–171.
26. Bae, S.J., Ni, L., Osinski, A., Tomchick, D.R., Brautigam, C.A., and Luo, X. (2017). SAV1 promotes Hippo kinase activation through antagonizing the PP2A phosphatase STRIPAK. Elife *6*, e30278.
27. Chen, R., Xie, R., Meng, Z., Ma, S., and Guan, K.L. (2019). STRIPAK integrates upstream signals to initiate the Hippo kinase cascade. Nat. Cell Biol. *21*, 1565–1577.
28. Gordon, J., Hwang, J., Carrier, K.J., Jones, C.A., Kern, Q.L., Moreno, C.S., Karas, R.H., and Pallas, D.C. (2011). Protein phosphatase 2a (PP2A) binds within the oligomerization domain of striatin and regulates the phosphorylation and activation of the mammalian Ste20-Like kinase Mst3. BMC Biochem. *12*, 54.
29. Jeong, B.C., Bae, S.J., Ni, L., Zhang, X., Bai, X.C., and Luo, X. (2021). Cryo-EM structure of the Hippo signaling integrator human STRIPAK. Nat. Struct. Mol. Biol. *28*, 290–299.
30. Seo, G., Han, H., Vargas, R.E., Yang, B., Li, X., and Wang, W. (2020). MAP4K Interactome Reveals STRN4 as a Key STRIPAK Complex Component in Hippo Pathway Regulation. Cell Rep. *32*, 107860.
31. Tang, Y., Chen, M., Zhou, L., Ma, J., Li, Y., Zhang, H., Shi, Z., Xu, Q., Zhang, X., Gao, Z., et al. (2019). Architecture, substructures, and dynamic assembly of STRIPAK complexes in Hippo signaling. Cell Discov. *5*, 3.
32. Tang, Y., Fang, G., Guo, F., Zhang, H., Chen, X., An, L., Chen, M., Zhou, L., Wang, W., Ye, T., et al. (2020). Selective Inhibition of STRN3-Containing PP2A Phosphatase Restores Hippo Tumor-Suppressor Activity in Gastric Cancer. Cancer Cell *38*, 115–128.
33. Zheng, Y., Liu, B., Wang, L., Lei, H., Pulgar Prieto, K.D., and Pan, D. (2017). Homeostatic Control of Hpo/MST Kinase Activity through Autophosphorylation-Dependent Recruitment of the STRIPAK PP2A Phosphatase Complex. Cell Rep. *21*, 3612–3623.
34. Decker, L., Desmarquet-Trin-Dinh, C., Taillebourg, E., Ghislain, J., Vallat, J.M., and Charnay, P. (2006). Peripheral myelin maintenance is a dynamic process requiring constant Krox20 expression. J. Neurosci. *26*, 9771–9779.

35. Ghislain, J., and Charnay, P. (2006). Control of myelination in Schwann cells: a Krox20 cis-regulatory element integrates Oct6, Brn2 and Sox10 activities. EMBO Rep. *7*, 52–58.

36. Le, N., Nagarajan, R., Wang, J.Y.T., Araki, T., Schmidt, R.E., and Milbrandt, J. (2005a). Analysis of congenital hypomyelinating Egr2Lo/Lo nerves identifies Sox2 as an inhibitor of Schwann cell differentiation and myelination. Proc. Natl. Acad. Sci. USA *102*, 2596–2601.

37. Le, N., Nagarajan, R., Wang, J.Y.T., Svaren, J., LaPash, C., Araki, T., Schmidt, R.E., and Milbrandt, J. (2005b). Nab proteins are essential for peripheral nervous system myelination. Nat. Neurosci. *8*, 932–940.

38. Mager, G.M., Ward, R.M., Srinivasan, R., Jang, S.W., Wrabetz, L., and Svaren, J. (2008). Active gene repression by the Egr2.NAB complex during peripheral nerve myelination. J. Biol. Chem. *283*, 18187–18197.

39. Zorick, T.S., Syroid, D.E., Arroyo, E., Scherer, S.S., and Lemke, G. (1996). The transcription factors SCIP and Krox-20 mark distinct stages and cell fates in Schwann cell differentiation. Mol. Cell. Neurosci. *8*, 129–145.

40. Zorick, T.S., Syroid, D.E., Brown, A., Gridley, T., and Lemke, G. (1999). Krox-20 controls SCIP expression, cell cycle exit and susceptibility to apoptosis in developing myelinating Schwann cells. Development *126*, 1397–1406.

41. Jung, J., Cai, W., Lee, H.K., Pellegatta, M., Shin, Y.K., Jang, S.Y., Suh, D.J., Wrabetz, L., Feltri, M.L., and Park, H.T. (2011). Actin polymerization is essential for myelin sheath fragmentation during Wallerian degeneration. J. Neurosci. *31*, 2009–2015.

42. Esposito, D., Pant, I., Shen, Y., Qiao, R.F., Yang, X., Bai, Y., Jin, J., Poulikakos, P.I., and Aaronson, S.A. (2022). ROCK1 mechano-signaling dependency of human malignancies driven by TEAD/YAP activation. Nat. Commun. *13*, 703.

43. Sabra, H., Brunner, M., Mandati, V., Wehrle-Haller, B., Lallemand, D., Ribba, A.S., Chevalier, G., Guardiola, P., Block, M.R., and Bouvard, D. (2017). β1 integrin-dependent Rac/group I PAK signaling mediates YAP activation of Yes-associated protein 1 (YAP1) via NF2/merlin. J. Biol. Chem. *292*, 19179–19197.

44. Talwar, S., Kant, A., Xu, T., Shenoy, V.B., and Assoian, R.K. (2021). Mechanosensitive smooth muscle cell phenotypic plasticity emerging from a null state and the balance between Rac and Rho. Cell Rep. *35*, 109019.

45. Zhao, B., Li, L., Wang, L., Wang, C.Y., Yu, J., and Guan, K.L. (2012). Cell detachment activates the Hippo pathway via cytoskeleton reorganization to induce anoikis. Genes Dev. *26*, 54–68.

46. Li, Y., Zhou, H., Li, F., Chan, S.W., Lin, Z., Wei, Z., Yang, Z., Guo, F., Lim, C.J., Xing, W., et al. (2015). Angiomotin binding-induced activation of Merlin/NF2 in the Hippo pathway. Cell Res. *25*, 801–817.

47. Yin, F., Yu, J., Zheng, Y., Chen, Q., Zhang, N., and Pan, D. (2013). Spatial organization of Hippo signaling at the plasma membrane mediated by the tumor suppressor Merlin/NF2. Cell *154*, 1342–1355.

48. Mindos, T., Dun, X.P., North, K., Doddrell, R.D.S., Schulz, A., Edwards, P., Russell, J., Gray, B., Roberts, S.L., Shivane, A., et al. (2017). Merlin controls the repair capacity of Schwann cells after injury by regulating Hippo/YAP activity. J. Cell Biol. *216*, 495–510.

49. Grove, M., Lee, H., Zhao, H., and Son, Y.J. (2020). Axon-dependent expression of YAP/TAZ mediates Schwann cell remyelination but not proliferation after nerve injury. Elife *9*, e50138.

50. Jeanette, H., Marziali, L.N., Bhatia, U., Hellman, A., Herron, J., Kopec, A.M., Feltri, M.L., Poitelon, Y., and Belin, S. (2021). YAP and TAZ regulate Schwann cell proliferation and differentiation during peripheral nerve regeneration. Glia *69*, 1061–1074.

51. Fan, F., He, Z., Kong, L.L., Chen, Q., Yuan, Q., Zhang, S., Ye, J., Liu, H., Sun, X., Geng, J., et al. (2016). Pharmacological targeting of kinases MST1 and MST2 augments tissue repair and regeneration. Sci. Transl. Med. *8*, 352ra108.

52. Lu, L., Li, Y., Kim, S.M., Bossuyt, W., Liu, P., Qiu, Q., Wang, Y., Halder, G., Finegold, M.J., Lee, J.S., and Johnson, R.L. (2010). Hippo signaling is a potent in vivo growth and tumor suppressor pathway in the mammalian liver. Proc. Natl. Acad. Sci. USA *107*, 1437–1442.

53. Wu, L.M.N., Deng, Y., Wang, J., Zhao, C., Wang, J., Rao, R., Xu, L., Zhou, W., Choi, K., Rizvi, T.A., et al. (2018). Programming of Schwann Cells by Lats1/2-TAZ/YAP Signaling Drives Malignant Peripheral Nerve Sheath Tumorigenesis. Cancer Cell *33*, 292–308.

54. Hwang, J., and Pallas, D.C. (2014). STRIPAK complexes: structure, biological function, and involvement in human diseases. Int. J. Biochem. Cell Biol. *47*, 118–148.

55. Kück, U., Radchenko, D., and Teichert, I. (2019). STRIPAK, a highly conserved signaling complex, controls multiple eukaryotic cellular and developmental processes and is linked with human diseases. Biol. Chem. *400*, 1005–1022.

56. Kück, U., and Stein, V. (2021). STRIPAK, a Key Regulator of Fungal Development, Operates as a Multifunctional Signaling Hub. J. Fungi *7*, 443.

57. Guo, Y., Zeng, Q., Brooks, D., and Geisbrecht, E.R. (2023). A conserved STRIPAK complex is required for autophagy in muscle tissue. Mol. Biol. Cell *34*, ar91.

58. Innokentev, A., Furukawa, K., Fukuda, T., Saigusa, T., Inoue, K., Yamashita, S.I., and Kanki, T. (2020). Association and dissociation between the mitochondrial Far complex and Atg32 regulate mitophagy. Elife *9*, e63694.

59. Sakuma, C., Saito, Y., Umehara, T., Kamimura, K., Maeda, N., Mosca, T.J., Miura, M., and Chihara, T. (2016). The Strip-Hippo Pathway Regulates Synaptic Terminal Formation by Modulating Actin Organization at the Drosophila Neuromuscular Synapses. Cell Rep. *16*, 2289–2297.

60. Sepp, K.J., and Auld, V.J. (2003). RhoA and Rac1 GTPases mediate the dynamic rearrangement of actin in peripheral glia. Development *130*, 1825–1835.

61. Aragona, M., Panciera, T., Manfrin, A., Giulitti, S., Michielin, F., Elvassore, N., Dupont, S., and Piccolo, S. (2013). A mechanical checkpoint controls multicellular growth through YAP/TAZ regulation by actin-processing factors. Cell *154*, 1047–1059.

62. Dupont, S., Morsut, L., Aragona, M., Enzo, E., Giulitti, S., Cordenonsi, M., Zanconato, F., Le Digabel, J., Forcato, M., Bicciato, S., et al. (2011). Role of YAP/TAZ in mechanotransduction. Nature *474*, 179–183.

63. Kurppa, K.J., and Westermarck, J. (2020). Good Guy in Bad Company: How STRNs Convert PP2A into an Oncoprotein. Cancer Cell *38*, 20–22.

64. Johnson, R., and Halder, G. (2014). The two faces of Hippo: targeting the Hippo pathway for regenerative medicine and cancer treatment. Nat. Rev. Drug Discov. *13*, 63–79.

65. Chen, M., Zhang, H., Shi, Z., Li, Y., Zhang, X., Gao, Z., Zhou, L., Ma, J., Xu, Q., Guan, J., et al. (2018). The MST4-MOB4 complex disrupts the MST1-MOB1 complex in the Hippo-YAP pathway and plays a pro-oncogenic role in pancreatic cancer. J. Biol. Chem. *293*, 14455–14469.

66. Sun, B., Zhong, F.J., Xu, C., Li, Y.M., Zhao, Y.R., Cao, M.M., and Yang, L.Y. (2021). Programmed cell death 10 promotes metastasis and epithelial-mesenchymal transition of hepatocellular carcinoma via PP2Ac-mediated YAP activation. Cell Death Dis. *12*, 849.

67. Wang, S., Englund, E., Kjellman, P., Li, Z., Ahnlide, J.K., Rodriguez-Cupello, C., Saggioro, M., Kanzaki, R., Pietras, K., Lindgren, D., et al. (2021). CCM3 is a gatekeeper in focal adhesions regulating mechanotransduction and YAP/TAZ signalling. Nat. Cell Biol. *23*, 758–770.

68. Li, A.X., Zeng, J.J., Martin, T.A., Ye, L., Ruge, F., Sanders, A.J., Khan, E., Dou, Q.P., Davies, E., and Jiang, W.G. (2023). Striatins and STRIPAK complex partners in clinical outcomes of patients with breast cancer and responses to drug treatment. Chin. J. Cancer Res. *35*, 365–385.

69. Migliavacca, J., Züllig, B., Capdeville, C., Grotzer, M.A., and Baumgartner, M. (2022). Cooperation of Striatin 3 and MAP4K4 promotes growth and tissue invasion. Commun. Biol. *5*, 795.

70. Owosho, A.A., Baker, E., Wood, C.B., and Jain, R. (2023). A novel STRN3::PRKD1 fusion in a cribriform adenocarcinoma of salivary gland

with high-grade transformation. Genes Chromosomes Cancer *62*, 624–628.

71. Tan, B., Long, X., Nakshatri, H., Nephew, K.P., and Bigsby, R.M. (2008). Striatin-3 gamma inhibits estrogen receptor activity by recruiting a protein phosphatase. J. Mol. Endocrinol. *40*, 199–210.
72. Tanti, G.K., Pandey, S., and Goswami, S.K. (2015). SG2NA enhances cancer cell survival by stabilizing DJ-1 and thus activating Akt. Biochem. Biophys. Res. Commun. *463*, 524–531.
73. Zhu, J., Tang, W., Fang, P., Wang, C., Gu, M., Yang, W., Pan, B., Wang, B., and Guo, W. (2024). STRN3 promotes tumour growth in hepatocellular carcinoma by inhibiting the hippo pathway. J. Cell Mol. Med. *28*, e18147.
74. Ghidinelli, M., Poitelon, Y., Shin, Y.K., Ameroso, D., Williamson, C., Ferri, C., Pellegatta, M., Espino, K., Mogha, A., Monk, K., et al. (2017). Laminin 211 inhibits protein kinase A in Schwann cells to modulate neuregulin 1 type III-driven myelination. PLoS Biol. *15*, e2001408.
75. Grove, M., Kim, H., Pang, S., Amaya, J.P., Hu, G., Zhou, J., Lemay, M., and Son, Y.J. (2024). TEAD1 is crucial for developmental myelination, Remak bundles, and functional regeneration of peripheral nerves. Elife *13*, e87394.
76. Laraba, L., Hillson, L., de Guibert, J.G., Hewitt, A., Jaques, M.R., Tang, T.T., Post, L., Ercolano, E., Rai, G., Yang, S.M., et al. (2023). Inhibition of YAP/TAZ-driven TEAD activity prevents growth of NF2-null schwannoma and meningioma. Brain *146*, 1697–1713.
77. Lopez-Anido, C., Poitelon, Y., Gopinath, C., Moran, J.J., Ma, K.H., Law, W.D., Antonellis, A., Feltri, M.L., and Svaren, J. (2016). Tead1 regulates the expression of Peripheral Myelin Protein 22 during Schwann cell development. Hum. Mol. Genet. *25*, 3055–3069.
78. Wang, J., Chen, H., Hou, W., Han, Q., and Wang, Z. (2023). Hippo Pathway in Schwann Cells and Regeneration of Peripheral Nervous System. Dev. Neurosci. *45*, 276–289.
79. Moore, S.M., Jeong, E., Zahid, M., Gawron, J., Arora, S., Belin, S., Sim, F., Poitelon, Y., and Feltri, M.L. (2024). Loss of YAP in Schwann cells improves HNPP pathophysiology. Glia *72*, 1974–1984.
80. Büssow, K., Schieich, C., Sievert, V., Harttig, U., Simon, B., Bork, P., Lehrach, H., and Heinemann, U. (2005). Structural genomics of human proteins–target selection and generation of a public catalogue of expression clones. Microb. Cell Fact. *4*, 21.
81. Skarnes, W.C., Rosen, B., West, A.P., Koutsourakis, M., Bushell, W., Iyer, V., Mujica, A.O., Thomas, M., Harrow, J., Cox, T., et al. (2011). A conditional knockout resource for the genome-wide study of mouse gene function. Nature *474*, 337–342.
82. Catignas, K.K., Frick, L.R., Pellegatta, M., Hurley, E., Kolb, Z., Addabbo, K., McCarty, J.H., Hynes, R.O., van der Flier, A., Poitelon, Y., et al. (2021). α_V integrins in Schwann cells promote attachment to axons, but are dispensable in vivo. Glia *69*, 91–108.
83. Poitelon, Y., Matafora, V., Silvestri, N., Zambroni, D., McGarry, C., Serghany, N., Rush, T., Vizzuso, D., Court, F.A., Bachi, A., et al. (2018). A dual role for Integrin $\alpha 6\beta 4$ in modulating hereditary neuropathy with liability to pressure palsies. J. Neurochem. *145*, 245–257.

STAR★METHODS

KEY RESOURCES TABLE

REAGENT or RESOURCE	SOURCE	IDENTIFIER
Antibodies		
Mouse anti-β-Actin	Santa Cruz	Cat# sc-47778; RRID: AB_626632
Mouse anti-β-tubulin	Sigma-Aldrich	Cat# T4026; RRID: AB_477577
Mouse anti-β-dystroglycan	Leica Biosystems	Cat# NCL-b-DG; RRID: AB_442043
Rabbit anti-Ccm3	Proteintech	Cat# 10294-2-AP; RRID: AB_2162153
Rabbit anti-Cdc42	Cell Signaling	Cat# 2462; RRID: AB_2078085
Rabbit anti-Egr2/Krox20	Gift generated by D. Meijer	N/A
Rabbit anti-GAPDH	Sigma-Aldrich	Cat# G9545; RRID: AB_796208
Rabbit anti-GFP	Proteintech	Cat# 50430-2-AP; RRID: AB_11042881
Rabbit anti-GST tag	Proteintech	Cat# 80006-1-RR; RRID: AB_2882936
Mouse anti-GST tag	Santa Cruz	Cat# sc-138; RRID: AB_627677
Rabbit anti-His tag	Cell Signaling	Cat# 2365S
Rabbit anti-His tag	Cell Signaling	Cat# 2366T
Goat anti-integrin α6	Santa Cruz	Cat# sc-6597; RRID: AB_2128041
Rat anti-integrin α6	Thermo Fisher Scientific	14-0495-85; RRID: AB_891484
Rabbit anti-integrin β1	Cell Signaling	Cat# 4706; RRID: AB_823544
Rat anti-integrin β4	Abcam	Cat# ab25254; RRID: AB_2129042
Rat anti-Ki67	Thermo Fisher Scientific	14-5698-80; RRID: AB_10853185
Mouse anti-Mob4/Phocein	Santa Cruz	Cat# sc-137229; RRID:AB_2250775
Rabbit anti-Mst1	Cell Signaling	Cat# 3682; RRID: AB_2144632
Rabbit anti-Mst2	Abcam	Cat# ab52641; RRID: AB_882734
Rabbit anti-p-Mst1/2	Proteintech	Cat# 28953-1-AP; RRID: AB_2918221
Chicken anti-neurofascin	R&D Systems	AF3235; RRID: AB_10890736
Rabbit anti-NF2	Cell Signaling	Cat# 6995; RRID:AB_10828709
Rabbit anti-p-NF2	Cell Signaling	Cat# 13281; RRID: AB_2650552
Rabbit anti-Oct6/Pou3f1	Gift generated by D. Meijer	N/A
Rabbit anti-Pak1	Cell Signaling	Cat# 2602; RRID: AB_330222
Rabbit anti-p-Pak1	Cell Signaling	Cat# 2601; RRID: AB_330220
Mouse anti-Rac1	EMD Millipore	Cat# 05–389; RRID: AB_309712
Mouse anti-Rac1	Cytoskeleton, Inc.	Cat# ARC03; RRID: AB_10709099
Rabbit anti-Rac1	Thermo Fisher Scientific	Cat# PA1-091; RRID: AB_2539856
Rabbit anti-Rac1	Proteintech	Cat# 24072-1-AP; RRID: AB_2879427
Rabbit anti-Sox10	Cell Signaling	Cat# 89356; RRID: AB_2792980
Mouse anti-StrepII tag	Thermo Fisher Scientific	Cat# MA5-37747; RRID: AB_2897671
Mouse anti-STRIP1	Origene	Cat# TA502314; RRID: AB_11126644
Mouse anti-striatin-1	Santa Cruz	Cat# sc-136084; RRID: AB_2271282
Rabbit anti-striatin-3	Atlas Antibodies	Cat# HPA004636; RRID: AB_1079940
Mouse anti-striatin-3	Novus Biologicals	Cat# NB110-74572; RRID: AB_1146988
Rabbit anti-striatin-4	GeneTex	Cat# GTX133282; RRID: AB_2886908
Mouse anti-Thy1.1	Bio-Rad	Cat# MCA045G
Rabbit anti-Yap	Cell Signaling	Cat# 4912; RRID: AB_2218911
Rabbit anti-Yap	Cell Signaling	Cat# 14074; RRID: AB_2650491
Rabbit anti-Yap/Taz	Cell Signaling	Cat# 8418; RRID: AB_10950494
Rabbit anti-p-Yap	Cell Signaling	Cat# 13008; RRID: AB_2650553

(*Continued on next page*)

Continued

REAGENT or RESOURCE	SOURCE	IDENTIFIER
Rabbit anti-p-Taz	Cell Signaling	Cat# 59971; RRID: AB_2799578
Donkey anti-rabbit 680	Li-Cor	Cat# 926-68073; RRID: AB_10954442
Goat anti-rabbit 800	Li-Cor	Cat# 926-32211; RRID: AB_621843
Goat anti-mouse IgG1 680	Li-Cor	Cat# 926-68050; RRID: AB_2783642
Goat anti-mouse IgG2b 800	Li-Cor	Cat# 926-32352; RRID: AB_2782999
Goat anti-rat 680	Li-Cor	Cat# 926-68029; RRID: AB_10715073
Goat anti-rat 800	Li-Cor	Cat# 926-32219; RRID: AB_1850025
Donkey anti-goat 680	Li-Cor	Cat# 926-68024; RRID: AB_10706168
Donkey anti-goat 800	Li-Cor	Cat# 926-32214; RRID: AB_621846
Donkey anti-rabbit HRP	Jackson ImmunoResearch	Cat# 711-035-152; RRID: AB_10015282
Goat anti-mouse IgG1 HRP	Thermo Fisher Scientific	Cat# A10551; RRID: AB_10561701
Goat anti-mouse IgG2a HRP	SouthernBiotech	Cat# 1080-05; RRID: AB_2734756
Goat anti-mouse IgG2b HRP	Thermo Fisher Scientific	Cat# M32407; RRID: AB_10563452
Goat anti-mouse Fc HRP	Sigma-Aldrich	Cat# A2554; RRID: AB_258008
Goat anti-mouse kappa light chain HRP	Jackson ImmunoResearch	Cat# 115-035-174; RRID: AB_2338512
Goat anti-rat light chain HRP	Jackson ImmunoResearch	Cat# 112-035-175; RRID: AB_2338140
Donkey anti-goat HRP	Jackson ImmunoResearch	Cat# 705-036-147; RRID: AB_2340392
Donkey anti-rabbit 488	Jackson ImmunoResearch	Cat# 711-545-152; RRID: AB_2313584
Donkey anti-rabbit Cy3	Jackson ImmunoResearch	Cat# 711-166-152; RRID: AB_2313568
Goat anti-rabbit 594	Invitrogen	Cat# A32740; RRID: AB_2762824
Goat anti-mouse IgG1 488	Thermo Fisher Scientific	Cat# A21121; RRID: AB_2535764
Goat anti-mouse IgG1 Cy3	Jackson ImmunoResearch	Cat# 115-165-205; RRID: AB_2338694
Donkey anti-chicken 488	Jackson ImmunoResearch	Cat# 703-545-155; RRID: AB_2340375
Donkey anti-rat Cy3	Jackson ImmunoResearch	Cat# 712-165-153; RRID: AB_2340667
Bacterial and virus strains		
DH5α E. Coli	Fischer Fisher Scientific	18265017
BL21(DE3) E. coli	Fischer Fisher Scientific	EC0114
Chemicals, peptides, and recombinant proteins		
Type I collagenase	Fischer Fisher Scientific	NC9633623
Poly-L-lysine	Sigma-Aldrich	P-5899
Cytosine β-D-arabinofuranoside hydrochloride	Sigma-Aldrich	C6645
High glucose DMEM	Thermo Fisher Scientific	11965-118
Fetal bovine serum	Thermo Fisher Scientific	10437028
L-glutamine	Thermo Fisher Scientific	25030-081
Penicillin + streptomycin	Thermo Fisher Scientific	15140-122
Neuregulin 1 (NRG1)	R&D Systems	396-HB-050
Forskolin	EMD Millipore	344270
Leibovitz's L-15 media	Thermo Fisher Scientific	11415064
Dispase II	Sigma-Aldrich	D4693
Laminin 111	Krackler/Sigma-Aldrich	L2020
Trypsin-EDTA	Thermo Fisher Scientific	15090046
Collagen I	Corning	354236
Glutathione magnetic agarose beads	Thermo Fisher Scientific	78601
GST-PAK-PBD	Cytoskeleton, Inc.	PAK01-A
Precision Red	Cytoskeleton, Inc.	ADV02
GDP	Sigma-Aldrich	G7637
GTPγS	Sigma-Aldrich	G8634

(*Continued on next page*)

Continued

REAGENT or RESOURCE	SOURCE	IDENTIFIER
GST-Rac1	Cytoskeleton, Inc.	RCG01-C
Protein G Dynabeads	Thermo Fisher Scientific	10004D
Phalloidin-488	Cytoskeleton, Inc.	PHDG1
His-Rac1	Cytoskeleton, Inc.	RC01-XL
His-human serum albumin	Abcam	ab217817
His-Strn3	MyBioSource	MBS1348331
Quick Load Taq-Mix 2x	New England Biolabs	M0271L
Trizol	Thermo Fisher Scientific	15596026
SYBR green qPCR Master Mix	Thermo Fisher Scientific	4309155
Taqman Universal PCR Master Mix	Thermo Fisher Scientific	4364338
Protease inhibitor cocktail	Sigma-Aldrich	P8340
Phosphatase inhibitor cocktail 2	Sigma-Aldrich	P5726
Phosphatase inhibitor cocktail 3	Sigma-Aldrich	P0044
4x Laemmli sample buffer	Bio-Rad	1610747
Bovine serum albumin	Sigma-Aldrich	A4161
Amarsham ECL Select	Cytiva	RPN2235
Triton X-100	Krackler/Sigma-Aldrich	T8787
DAPI	Krackler/Sigma-Aldrich	45-D9542-5MG
Vectashield	Vector Laboratories	H-1000-10
Rhodamine-phalloidin	Cytoskeleton, Inc.	PHDR1
Critical commercial assays		
Duolink *In Situ* Detection Reagents Red	Sigma-Aldrich	DUO92008
Superscript III	Thermo Fisher Scientific	18080051
BCA assay	Thermo Fisher Scientific	23225
Deposited data		
Raw proteomics data	OSF Registries	https://osf.io/syqn6/
Experimental models: Organisms/strains		
Striatin-1 floxed mice	Mutant Mouse Resources & Research Centers (MMRRC)	$Strn^{tm1a(KOMP)Wtsi}$/MbpMmucd
Striatin-3 floxed mice	Mutant Mouse Resources & Research Centers (MMRRC)	$Strn3^{tm1a(KOMP)Wtsi}$
Striatin-4 floxed mice	European Mutant Mouse Archive	$Strn4^{tm1a(EUCOMM)Hmgu}$/Ph
Rac1 floxed mice	Nodari et al.[6]	RRID: IMSR_JAX:005550
Mpz-Cre	Our laboratory[22]	RRID: IMSR_JAX:017927
Oligonucleotides		
Primers for genotyping, see Table S1	This paper	N/A
Primers for qPCR, see Table S2	This paper	N/A
Recombinant DNA		
pQStrep2-PREI3 (His-Mob4-StrepII)	Bussow et al.[80]	Cat# 31592; RRID: Addgene_31592
Software and algorithms		
Q-Capture Pro	QImaging, Inc	v7.0.4324.5
PTGui	New House Internet Services BV	v10
Fiji/ImageJ	ImageJ	v1.52h
Image Studio Lite	Li-Cor	V5.2
Image Lab	Bio-Rad	V6.0
LAS AF	Leica	v2.7.9723.3
Prism	GraphPad	v8.0.2

EXPERIMENTAL MODEL AND STUDY PARTICIPANT DETAILS

Animal models

All animal experiments were approved by the Institutional Animal Care and Use Committee (IACUC) of Roswell Park Comprehensive Cancer Center (RPCCC) and the State University of New York (SUNY) University at Buffalo protocols UB1188M and UB1194M. Animals were housed in sex-segregated, individually ventilated cages with a maximum of five adult mice per cage. Food and water were provided *ad libitum* and rooms were maintained at a 12-h light/dark cycle. MPZ-Cre, Strn1-floxed, Strn3-floxed, Strn4-floxed, and Rac1-floxed mice kept in a C57BL/6 background strain were used in this study.[6,22] All three striatin lines were generated as part of the UC Davis Knockout Mouse Project (KOMP).[81] Striatin-1 floxed and striatin-3 floxed mice were obtained from the Mutant Mouse Resources & Research Centers (MMRRC) while striatin-4 floxed mice were obtained from the European Mutant Mouse Archive (EMMA) node at the Institute of Molecular Genetics ASCR. For single Schwann cell knockout (SCKO) animals, mice carrying one or two floxed alleles but no MPZ-Cre were used as controls. For double SCKO (dSCKO) animals, mice carrying three or four floxed alleles but no MPZ-Cre were used as controls. In general, all experiments included 3–8 biological replicates per genotype. No animals were excluded from this study.

Cell culture

Primary rat SCs (rSC) were isolated from P3 rat sciatic nerves. Nerves were dissected, dissociated with 130 U/ml type I collagenase (Fischer Scientific NC9633623), and cells were then plated on poly-L-lysine (PLL, Sigma-Aldrich P-5899)-coated tissue culture dishes. Plates were coated with PLL by incubation with 0.01 mg/mL PLL in water for 30 min at room temperature followed by washing with phosphate buffered saline (PBS). Contaminant fibroblasts were killed to achieve 99–100% rSC culture purity by treatment with cytosine β-D-arabinofuranoside hydrochloride (Sigma-Aldrich C6645) followed by two treatments of mouse anti-Thy1.1 monoclonal antibody (Bio-Rad MCA045G) and rabbit complement. Cultures were limited to five passages in media containing high glucose DMEM (Thermo Fisher Scientific 11965-118) supplemented with 10% fetal bovine serum (FBS, Thermo Fisher Scientific 10437028), 2 mM L-glutamine (Thermo Fisher Scientific 25030-081), 100 U/mL penicillin +100 μg/mL streptomycin (Thermo Fisher Scientific 15140-122), 2 ng/mL NRG1 (R&D Systems 396-HB-050), and 2 μM forskolin (EMD Millipore 344270). Primary mouse SCs (mSC) were prepared from pooled sciatic nerves of adult mice aged P45-60. Nerves were dissected, placed in ice-cold Leibovitz's L-15 media (Thermo Fisher Scientific 11415064) supplemented with 100 U/mL penicillin +100 μg/mL streptomycin, and stripped of epineurium and other contaminant tissues. Cleaned nerve explants were then transferred into tissue culture dishes (6–8 nerves/35 mm dish) containing nerve explant/mSC media (identical to rSC media except for NRG1 increased to 10 ng/mL). Nerve explants were incubated at 37°C, 5% CO_2 for 7 days with media changes every other day to allow for formation of repair SCs. Cells were then enzymatically dissociated by placing explants in L-15 media containing 2.5 mg/mL dispase II (Sigma-Aldrich D4693), 130 U/ml type I collagenase, and 5 mM HEPES while incubating at 37°C for 3 h with gentle rocking at 40 rpm. Tissue was then mechanically dissociated using fire-polished glass pipettes followed by passage through a 70 μM cell strainer. The cell suspension was then centrifuged, the resulting pellet was resuspended in mSC media, and cells were plated on tissue culture plates coated with PLL and laminin 111 (Krackler/Sigma-Aldrich L2020). Plates were coated with PLL+laminin by incubation with 0.01 mg/mL PLL in water for 30 min at room temperature, washing with PBS, incubation with 0.01 mg/mL laminin 111 in PBS for 1 h at room temperature, incubation with mSC media for 30 min at room temperature, and then washing with PBS. Resultant mSC cultures were passaged once as appropriate for each experiment. Mouse embryonic fibroblasts (MEFs) were isolated from E12.5–14.5 mouse embryos. Embryos were dissected from pregnant female mice and placed in a tissue culture dish with ice-cold PBS. Yolk sac, head, heart, and liver were removed. Embryos were then placed into a fresh tissue culture dish with 0.25% trypsin-EDTA (Thermo Fisher Scientific 15090046) in PBS, minced, incubated at 37°C for 10 min, and then pipetted several times to obtain a near single-cell suspension. Cells were transferred to a dish coated with collagen I (Corning 354236) and allowed to adhere by incubating overnight at 37°C, 5% CO_2 in MEF/HEK media (high glucose DMEM supplemented with 10% FBS and 100 U/mL penicillin +100 μg/mL streptomycin). Collagen coating was performed by incubating dishes with 0.01 mg/mL collagen I in PBS for 1 h at room temperature. After adhering overnight, residual debris was washed away wish PBS. MEFs were limited to 10 passages.

METHOD DETAILS

Rac1 activity assay

For each 400 μg tissue sample, 5 μL of settled (20 μL of slurry) glutathione magnetic agarose beads (Thermo Fisher Scientific 78601) were first washed 3x with 800 μL Rac1 lysis buffer (20 mM Tris-HCl pH 7.5, 150 mM NaCl, 1% Triton X-100, 10 mM $MgCl_2$, 10 mM NaF, and 1:100 protease inhibitor cocktail) and then resuspended in 800 μL Rac1 lysis buffer with 10 μg GST-PAK-PBD (Cytoskeleton, Inc. PAK01-A). GST-PAK-PBD was conjugated to beads by rotating for 1 h at room temperature, followed by washing 3x in 800 μL Rac1 wash buffer and then resuspending in 300 μL cold Rac1 wash buffer on ice. Pulverized sciatic nerves and brachial plexuses were prepared as described in supplemental methods. Pulverized tissue was lysed with Rac1 lysis buffer and centrifuged at 13,200 rcf for 1 min at 4°C. Protein concentration of the supernatant was quantified by Precision Red assay (Cytoskeleton, Inc. ADV02). For GDP and GTP-charged controls, 100 μg of tissue lysate was incubated with 2 μL 0.5 M EDTA and either 5 μL 20 mM GDP (Sigma-Aldrich G7637) or 5 μL 20 mM GTPγS (Sigma-Aldrich G8634) for 15 min at 37°C. GDP/GTP control charge reactions

were stopped by adding 6 μL 1M $MgCl_2$. To pull down active Rac1, 400 μg of tissue lysate (or 100 μg for GDP/GTP-charged controls) was added to GST-PAK-PBD-conjugated beads. Total volume per sample was brought to 800 μL with cold Rac1 lysis buffer and samples were rotated for 1 h at 4°C. Lysate was removed and beads were washed with 800 μL with cold Rac1 lysis buffer. Rac1 lysis buffer was removed, samples were centrifuged at 1,000 rcf for 5 s at 4°C, and then residual buffer was removed. Samples were eluted by boiling in 40 μL 2x Laemmli buffer for 10 min at 95°C. Samples were then analyzed by western blot as described in supplemental methods.

Rac1 pull-down assay

For each 500 μg tissue sample, 5 μg of GST-Rac1 (Cytoskeleton, Inc. RCG01-C) was charged with GDP or GTPγS by incubating for 20 min at 37°C in 100 μL GST pull-down buffer (20 mM Tris-HCl pH 7.4, 150 mM NaCl, 0.1% Triton X-100, 10 mM $MgCl_2$, and 1:100 protease inhibitor cocktail) containing 20 mM EDTA and1 mM of either GDP or GTPγS. The charge reaction was stopped by adding an additional 2 μL 1M $MgCl_2$. For each sample, 5 μl settled glutathione beads (20 μL bead slurry) were rinsed 3x in 800 μL GST pull-down buffer and then resuspended in 400 μL GST pull-down buffer. To conjugate GST-Rac1-GDP/GTPγS to the beads, each ~100 μl charge reaction was combined with a 400 μL washed bead suspension and rotated for 1 h at 4°C, washed 3x with 800 μL cold GST pull-down buffer, and then resuspended in 300 μL GST pull-down buffer. GST-Rac1-GDP/GTPγS-conjugated beads were then combined with 500 μg tissue lysed in Rac1 lysis buffer as described above and rotated for 1 h at 4°C. Samples were rinsed 3x with 800 μL cold GST pull-down buffer, centrifuged at 1,000 rcf for 5 s at 4°C, and then residual buffer was removed. Samples were either eluted by boiling in 40 μL 2x Laemmli buffer for 10 min at 95°C for analysis by western blot as described above or frozen and shipped to colleagues for analysis by tandem mass spectroscopy (MS/MS). For MS/MS analysis, samples were digested with trypsin to generate tryptic peptides. The Welch difference was calculated as the log2-fold change in protein enrichment between Rac1-GDP and Rac1-GTP fractions. A false discovery rate (FDR) = 0.5 was used as the cutoff value to declare a protein specifically enriched in either fraction.

Co-immunoprecipitation (coIP)

Rat SCs (rSC) were cultured in rSC media (described in supplemental methods) on uncoated tissue culture dishes until approximately 80% confluent.[82] Cells were then washed with cold PBS and lysed in ice-cold IP lysis buffer (PBS +1% NP-40 + 1 mM EDTA +1:100 protease inhibitor cocktail). Lysate protein concentration was quantified by BCA assay and 1 mg of protein was combined with 0.25 μg of either rabbit anti-Rac1 experimental antibody (Thermo Fisher Scientific PA1-091) or rabbit anti-GFP isotype control antibody (Proteintech 50430-2-AP) for each coIP reaction. Samples were then rotated overnight at 4°C to facilitate antibody-antigen binding. Protein G Dynabeads (Thermo Fisher Scientific 10004D) were prepared by rinsing 10.4 μL bead slurry (0.3125 mg beads) per reaction with IP lysis buffer.[83] The antibody-antigen complex was then captured by adding rinsed beads to each coIP reaction and rotating for 1 h at 4°C. Samples were then washed 3x 5 min at 4°C in IP lysis buffer, transferred to a fresh microcentrifuge tube during the final wash, and then eluted by boiling in 40 μL 2x Laemmli buffer for 10 min at 95°C for analysis by western blot (described in supplemental methods).

Proximity ligation assay

Cells were plated on 96-well plates at 8000 cells/well and allowed to adhere overnight at 37°C, 5% CO_2. rSCs were plated on wells coated with PLL + laminin 111 (as described above), while MEF and human embryonic kidney (HEK) cells were plated on PLL + collagen I. The procedure for PLL + collagen I coating was identical to that for PLL + laminin 111 coating, except that laminin 111 was substituted for collagen I diluted to 0.01 mg/mL in PBS. rSCs were incubated in rSC media while MEFs and HEKs were incubated in MEF/HEK media (described above). Cells were fixed by incubating with 4% PFA in PBS at room temperature for 20 min. Cells were then permeabilized and stained for F-actin by incubating with phalloidin-488 1:200 (Cytoskeleton, Inc. PHDG1) in PBS and 0.5% Triton X-100 for 1 h at room temperature. Samples were then blocked and nuclei were stained by incubating with DAPI in Duolink blocking solution (Duolink *In Situ* Detection Reagents Red kit, Sigma-Aldrich DUO92008) for 1 h at room temperature. Samples were then immunolabeled by incubating with primary antibodies in Duolink antibody diluent overnight at 4°C, washing 3x in Duolink wash buffer A, incubating with Duolink secondary antibody probes (anti-rabbit Plus and anti-mouse Minus) each diluted 1:5 in Duolink antibody diluent overnight at 37°C, and then washing 3x in Duolink wash buffer A. Duolink probes were ligated by incubating with Duolink ligase enzyme diluted 1:40 in Duolink ligase buffer for 1 h at 37°C and then washing 3x in Duolink wash buffer A. Ligated DNA probes were amplified by rolling circle amplification (RCA) by incubation with Duolink polymerase diluted 1:80 in Duolink amplification buffer overnight at 37°C. Samples were then washed 3x with Duolink wash buffer B, 1x with 1:100 Duolink wash buffer B, 1x with PBS, and then imaged in PBS. The following primary antibodies were used: mouse anti-striatin-3 (Novus Biologicals NB110-74572) and rabbit anti-Rac1 (Proteintech 24072-1-AP). Immunofluorescent images were acquired as described above.

Dot blot

For each charge reaction, bait proteins His-Rac1 (Cytoskeleton, Inc. RC01-XL) or His-human serum albumin (His-HSA, Abcam ab217817) negative control were diluted to 10 μM in 140 μL PD6 buffer (5 mM Tris-HCl pH 7.4, 12.5 mM $NaCl_2$, 0.25 mM $MgCl_2$, and 1:400 protease inhibitor cocktail) containing 1 mM GDP or GTPγS and incubated for 20 min at 37°C. Nitrocellulose membranes were labeled in pencil with a 1 × 1 cm grid pattern, and 2 μL dots of a serial dilution of His-Rac1-GDP/GTPγS or

His-HSA-GDP/GTPγS charge reactions were dotted along the membranes. The serial dilution was as follows: blank charge reaction, 2.5 pmol, 5 pmol, 10 pmol, and 20 pmol. Rows along each membrane alternated between His-Rac1 and His-HSA dots, while membranes were separated by GDP vs. GTPγS charge state. After laying protein dots, membranes were allowed to air dry for 15 min at room temperature. Membranes were rehydrated in TBS-T + 1 mM $MgCl_2$, washed 3x with TBS-T + 1 mM $MgCl_2$, and then blocked in 5% BSA in TBS-T + 1 mM $MgCl_2$ for 1 h at room temperature. Membranes were then incubated with prey proteins GST-PAK-PBD, His-Strn3 (MyBioSource MBS1348331), or His-Mob4-StrepII (prepared from Addgene expression plasmid # 31592, http://n2t.net/addgene:31592, RRID: Addgene_31592, a gift from Konrad Büssow) diluted to 100 nM in 5% BSA in TBS-T + 1 mM $MgCl_2$ overnight at 4°C[70]. Plasmid for His-Mob4-StrepII expression was stored in DH5α E. coli (Thermo Fisher Scientific 18265017) while protein expression was accomplished using BL21(DE3) E. coli (Thermo Fisher Scientific EC0114). Dot blot membranes were then washed 3x with TBS-T and then immunolabelled and imaged according to a slightly modified version of the western blot protocol described in supplemental methods. Differences included reducing the primary antibody incubation time to 1 h and performing the secondary antibody incubation at 4°C.

Genotyping

Genomic DNA was used for genotyping as follows. Thermocycler conditions for all genotypes were 94°C for 5 min, (94°C for 15s, 65°C-56°C [-1°C per cycle] for 30s, 72°C for 40s) for 10 cycles, (94°C for 15s, 55°C for 30s, 72°C for 40s) for 30 cycles, 72°C for 5 min. PCR reaction mixtures were prepared with Quick Load Taq-Mix 2x (New England Biolabs M0271L). For MPZ-Cre, primers were A: 5′- CCACCACCTCTCCATTGCAC-3′, AS2: 5′- GCTGGCCCAAATGTTGCTGG-3′, 5MP2: 5′- TGTTGGCAACTTTGGAT GTGT-3′, and P3P: 5′- TCAGCCAAGCCTTACCTTACT-3′, yielding bands of ∼203 bp (internal control) and ∼450 bp (transgene). For Strn1-floxed, primers were Strn1-F: 5′- TGAATTATTGGAGTTTTGTTTCAGACC-3′ and Strn1-ttR: 5′- GCACAGACAGACCTTCA TGCTAACC-3′, yielding bands of ∼531 bp (WT) and ∼630 bp (floxed). For Strn3-floxed, primers were Strn3-F: 5′- ACCACAAA ACAAGTGGTAGCTGAACC-3′ and Strn3-ttR: 5′- TGAAGGTGGTAGGAATACAGAATAGCC-3, yielding bands of ∼684 bp (WT) and ∼818bp (floxed). For Strn4 floxed, primers were Strn4-Fwd-3: 5′-CAGAGCAGCTGCTTGGCATAGAG-3′ and Strn4-Rev-3: 5′-CA CAACCGTGCACACTGGTGC-3′, yielding bands of ∼645bp (WT) and ∼733bp (floxed). For Rac1-floxed, primers were Rac1-1: 5′- ATTTTGTGCCAAGGACAGTGACAAGCT-3′, Rac1-2: 5′- GAAGGAGAAGAAGCTGACTCCCATC-3′, and Rac1-3: 5′- CAGCCACAGG CAATGACAGATGTTC-3′, yielding bands of ∼175bp (recombined), ∼300bp (WT), and ∼333bp (floxed).

Morphological assessment

Mice were euthanized at the specified ages and then sciatic nerves were dissected, fixed in 2% glutaraldehyde, and stored at 4°C until processing. Nerves were then post-fixed in 1% osmium tetroxide, dehydrated by serial incubations of increasing ethanol concentration, and embedded in Epon resin with a transition solvent of propylene oxide. Embedded samples were then cut as semithin sections (1 μm) and stained with 2% toluidine blue for light microscopy or as ultrathin sections (80–85 nm) and stained with uranyl acetate and lead citrate for electron microscopy. For analysis of g-ratio, myelinated fiber density, total myelinated fibers per nerve, and nerve cross-sectional area, images were acquired with the 100x objective of a Leica DM6000 microscope and Q-Capture Pro V7.0.4324.5 software (QImaging, Inc). G-ratio was subsequently calculated using semi-automated Leica QWin software (Leica Microsystem). For myelinated fiber density, total myelinated fibers per nerve, and nerve cross-sectional area, the 100x images were stitched together with PTGui software v.10 (New House Internet Services BV) to assemble a full nerve cross-section. Morphological measurements were made using Fiji software v1.52h (ImageJ). Transmission electron micrographs at 2900x magnification were acquired and then analyzed by Fiji software to quantify unsorted axon bundle size, axons per unsorted bundle, % amyelinated axons, and % axons with myelin abnormalities (infoldings, outfoldings, and decompaction).

RNA extraction and RT-qPCR analysis

Sciatic nerves and brachial plexuses were dissected at the indicated ages, contaminant tissue was removed, samples were snap frozen in liquid nitrogen, and then stored at −80°C. Nerves were then pulverized, total RNA was isolated using Trizol (Thermo Fisher Scientific 15596026), and cDNA was prepared using the Superscript III kit (Thermo Fisher Scientific 18080051). For each reverse transcription reaction, 350 μg RNA and 5 μM of oligo(dT) were used. For SYBR qPCR reactions, SYBR green qPCR Master Mix (Thermo Fisher Scientific 4309155) was used for the following primer sets. For Itga6, primers were Fwd: 5′- CCTGAAAGAAAA TACCAGACTCTCA-3′, Rev: 5′-GGAACGAAGAACGAGAGAGG-3’. For Itgb1, primers were Fwd: 5′-CAACCACAACAGCTGCTTC TAA-3′, Rev: 5′-TCAGC CCTCTTGAATTTTAATGT-3’. For Itgb4, primers were Fwd: 5′-CTTGGTCGCCGTCTGGTA-3′, Rev: 5′-TCGAAGGACACTACCCCACT-3’. For Dag1, primers were Fwd: 5′-CTGCTGCTGCTCCCTTTC-3′, Rev: 5′-GCAGTGTTGAAAACCT TATCTTCC-3’. For GAPDH, primers were Fwd: 5′-CAACTCCCTCAAGATTGTCAGCAA-3′, Rev: 5′-GGCATGGACTGTGGTCAT GA-3’. For Taqman qPCR reactions, Taqman Universal PCR Master Mix (Thermo Fisher Scientific 4364338) was used for the following Thermo Fisher Scientific Taqman assay gene probes: Ccm3 (Mm00727342_s1), Egr2/Krox20 (Mm00456650_m1), GAPDH (Mm99999915_g1), Mst1 (Mm00451755_m1), Mst2 (Mm00490480_m1), Mob4 (Mm00481145_m1), Oct6/Pou3f1 (Mm00843 534_s1), Strip1 (Mm00463714_m1), Strn1 (Mm00448910_m1), Strn3 (Mm00453492_g1), Strn4 (Mm00467125_m1), Taz (Mm0128 9583_m1), and Yap (Mm01143263_m1). SYBR and Taqman qPCR assays were normalized to GAPDH reference gene. All qPCR

assays were performed using a Bio-Rad CFX96/384 RT-qPCR machine with the following thermocycler protocol: 95°C for 10 min following by 40 cycles of (95°C for 15 s and 60°C for 1 min). Data were analyzed using threshold cycle (Ct) and 2(−ΔΔCt) with the average expression of WT control animals normalized to 1.

Western blot

Sciatic nerves and brachial plexuses were dissected at the indicated ages, contaminant tissue was removed, samples were snap frozen in liquid nitrogen, and then stored at −80°C. Nerves were then pulverized and lysed in RIPA lysis buffer (50 mM Tris pH 7.4, 150mM, NaCl, 1% IGEPAL CA-630, 0.1% SDS, 0.5% sodium deoxycholate, 5mM EDTA, 1mM EGTA, 1 mM NaF, 1:100 protease inhibitor cocktail (Sigma-Aldrich P8340), 1:100 phosphatase inhibitor cocktail 2 (Sigma-Aldrich P5726), and 1:100 phosphatase inhibitor cocktail 3 (Sigma-Aldrich P0044)). Cells were lysed directly from plates using RIPA lysis buffer. Following lysis, samples were sonicated for two cycles of 30 s at 70% power and centrifuged at 13,200 rcf for 15 min at 4°C. Protein concentration of the supernatant was quantified by BCA assay (Thermo Fisher Scientific 23225). Loading samples for each experiment were prepared at equal concentrations by diluting supernatant with RIPA lysis buffer and 4x Laemmli sample buffer (Bio-Rad 1610747, supplemented with β-mercaptoethanol as per manufacturer's instructions). Loading samples were electrophoresed through an SDS-polyacrylamide hydrogel and then transferred onto a PVDF membrane. Membranes were then blocked with 5% bovine serum albumin (BSA, Sigma-Aldrich A4161) in TBS-T (1x tris-buffered saline +0.1% Tween 20) and immunolabelled with primary antibody in 5% BSA in TBS-T overnight at 4°C with gentle rocking. Next, membranes were washed with TBS-T, incubated with secondary antibody in 5% BSA in TBS-T for 1 h at room temperature, and washed again with TBS-T. The following primary antibodies were used: mouse anti-β-Actin 1:1000 (Santa Cruz sc-47778), mouse anti-β-tubulin 1:2000 (Sigma-Aldrich T4026), mouse anti-β-dystroglycan 1:500 (Leica Biosystems NCL-b-DG), rabbit anti-Ccm3 1:250 (Proteintech 10294-2-AP), rabbit anti-Cdc42 1:250 (Cell Signaling 2462), rabbit anti-Egr2/Krox20 1:500 (kindly shared by D. Meijer), rabbit anti-GAPDH 1:10,000 (Sigma-Aldrich G9545), rabbit anti-GST tag 1:1000 (Proteintech 80006-1-RR), mouse anti-GST tag 1:1000 (Santa Cruz sc-138), rabbit anti-His tag 1:1000 (Cell Signaling 2365S), rabbit anti-His tag 1:50,000 (Cell Signaling 2366T), goat anti-integrin α6 1:250 (Santa Cruz sc-6597), rabbit anti-integrin β1 1:250 (Cell Signaling 4706), rat anti-integrin β4 1:250 (Abcam ab25254), mouse anti-Mob4/Phocein 1:250 (Santa Cruz sc-137229), rabbit anti-Mst1 1:500 (Cell Signaling 3682), rabbit anti-Mst2 1:500 (Abcam ab52641), rabbit anti-p-Mst1/2 1:250 (Proteintech 28953-1-AP), rabbit anti-NF2 1:500 (Cell Signaling 6995), rabbit anti-p-NF2 1:500 (Cell Signaling 1328), rabbit anti-Oct6/Pou3f1 1:500 (kindly shared by D. Meijer), rabbit anti-Pak1 1:500 (Cell Signaling 2602), rabbit anti-p-Pak1 1:500 (Cell Signaling 2601), mouse anti-Rac1 1:250 (EMD Millipore 05–389), mouse anti-Rac1 1:250 (Cytoskeleton, Inc. ARC03), rabbit anti-Rac1 1:500 (Thermo Fisher Scientific PA1-091), rabbit anti-Rac1 1:500 (Proteintech 24072-1-AP), rabbit anti-Sox10 1:250 (Cell Signaling 89356), mouse anti-StrepII tag 1:250 (Thermo Fisher Scientific MA5-37747), mouse anti-STRIP1 1:250 (Origene TA502314), mouse anti-striatin-1 (Santa Cruz sc-136084), rabbit anti-striatin-3 1:100 (Atlas Antibodies HPA004636), mouse anti-striatin-3 (Novus Biologicals NB110-74572), rabbit anti-striatin-4 (GeneTex GTX133282), rabbit anti-Yap 1:250 (Cell Signaling 4912), rabbit anti-Yap 1:250 (Cell Signaling 14074), rabbit anti-Yap/Taz 1:250 (Cell Signaling 8418), rabbit anti-p-Yap 1:250 (Cell Signaling 13008), rabbit anti-p-Taz 1:250 (Cell Signaling 59971). The following secondary antibodies were used: donkey anti-rabbit 680 1:20,000 (Li-Cor 926-68073), goat anti-rabbit 800 1:20,000 (Li-Cor 926-32211), goat anti-mouse IgG1 680 (Li-Cor 926-68050), goat anti-mouse IgG2b 800 1:20,000 (Li-Cor 926-32352), goat anti-rat 680 1:20,000 (Li-Cor 926-68029), goat anti-rat 800 1:20,000 (Li-Cor 926-32219), donkey anti-goat 680 1:20,000 (Li-Cor 926-68024), donkey anti-goat 800 1:20,000 (Li-Cor 926-32214), donkey anti-rabbit HRP 1:20,000 (Jackson ImmunoResearch 711-035-152), goat anti-mouse IgG1 HRP 1:20,000 (Thermo Fisher Scientific A10551), goat anti-mouse IgG2a HRP 1:20,000 (SouthernBiotech 1080-05), goat anti-mouse IgG2b HRP 1:20,000 (Thermo Fisher Scientific M32407), goat anti-mouse Fc HRP 1:20,000 (Sigma-Aldrich A2554), goat anti-mouse kappa light chain HRP 1:20,000 (Jackson ImmunoResearch 115-035-174), goat anti-rat light chain HRP 1:20,000 (Jackson ImmunoResearch 112-035-175), donkey anti-goat HRP 1:20,000 (Jackson ImmunoResearch 705-036-147). Membranes were either imaged directly with Li-Cor Odyssey CLx infrared imaging system or imaged using a ChemiDoc XRS system after developing with Amarsham ECL Select (Cytiva RPN2235). Bands were quantified with either Image Studio Lite 5.2 software (Odyssey) for infrared blots or Image Lab 6.0 software (Bio-Rad) for chemiluminescent blots. GAPDH was used as a loading control.

Immunofluorescence

Samples were first fixed by incubation with 4% paraformaldehyde (PFA) in PBS on ice for 30 min (nerves) or 20 min (cells). Nerve samples were then cryprotected by incubating in 20% sucrose in PBS overnight at 4°C, embedded in tissue freezing medium, and cut into 8 μM thick sections onto glass slides. Samples were blocked and permeabilized by incubation with blocking buffer 1 (20% FBS, 1% BSA, and 1% Triton X-100 (Krackler/Sigma-Aldrich T8787) in PBS) for 1 h at room temperature. Immunolabeling of samples was accomplished by incubation with primary antibodies in blocking buffer overnight at 4°C, incubation with secondary antibodies for 1 h at room temperature, counterstaining with DAPI (Krackler/Sigma-Aldrich 45-D9542-5MG) for 10 min at room temperature, and mounting slides or coverslips with Vectashield (Vector Laboratories H-1000-10). Where indicated, rhodamine-conjugated phalloidin 1:200 (Cytoskeleton, Inc. PHDR1) was incubated with secondary antibodies to stain for F-actin. Nerves used for labeling Sox10 and Ki67 were flash frozen fresh (unfixed) in tissue freezing medium, then sectioned into 8 μM thick sections onto glass slides. Samples were then post-fixed by incubation with 4% PFA in PBS for 8 min. Samples were then permeabilized by incubation in cold methanol for 3 min and blocked by incubation in blocking buffer 2 (2% normal goat serum, 3% BSA, 0.5% Triton X-100 in PBS)

for 1 h at room temperature. Immunolabeling and slide preparation then proceeded as described above, with the exception that antibodies were diluted in blocking buffer 2. The following primary antibodies were used: rabbit anti-striatin-3 1:100 (Atlas Antibodies HPA004636), mouse anti-striatin-3 (Novus Biologicals NB110-74572), rabbit anti-Sox10 1:100 (Cell Signaling 89356), chicken anti-neurofascin 1:1000 (R&D Systems AF3235), rat anti-integrin α6 1:100 (Thermo Fisher Scientific 14-0495-85), and rat anti-Ki67 1:300 (Thermo Fisher Scientific 14-5698-80). The following secondary antibodies were used: donkey anti-rabbit 488 1:1000 (Jackson ImmunoResearch 711-545-152), donkey anti-rabbit Cy3 1:500 (Jackson ImmunoResearch 711-166-152), goat anti-rabbit 594 1:500 (Invitrogen A32740), goat anti-mouse IgG1 488 1:1000 (Thermo Fisher Scientific A21121), goat anti-mouse IgG1 Cy3 1:500 (Jackson ImmunoResearch 115-165-205), donkey anti-chicken 488 1:1000 (Jackson ImmunoResearch 703-545-155), donkey anti-rat Cy3 1:500 (Jackson ImmunoResearch 712-165-153). Immunofluorescence images were acquired using a Leica SP5II confocal microscope running LAS AF 2.7.9723.3 software.

QUANTIFICATION AND STATISTICAL ANALYSIS

All data collection and analyses were performed blind to the experimental conditions and animal genotype where applicable. No data were excluded from the analyses. Power analysis was not performed, but our sample sizes reflect those generally accepted. Figure legends report the statistical test used in each experiment. Graphs are presented as the mean average ±SEM. Statistical trends were reported as values where $0.05 < p < 0.1$, while statistical significance was reported as values where $p < 0.05$. Data were analyzed using GraphPad Prism software v8.0.2.